NCAR-TN/STR-98
NCAR TECHNICAL NOTE

August 1974

Modification of Aerosol Size Distributions in the Troposphere

I. H. Blifford
National Center for Atmospheric Research

J. W. Burgmeier
Department of Mathematics
University of Vermont

C. E. Junge
Max Planck Institute for Chemistry
Mainz, Germany

ATMOSPHERIC QUALITY AND MODIFICATION DIVISION

NATIONAL CENTER FOR ATMOSPHERIC RESEARCH
BOULDER, COLORADO

PREFACE

This work is an extension of the study of tropospheric aerosols begun in 1964 by Christian Junge. The model presented for description of these aerosols contains more processes than Junge originally considered and the model was allowed to run longer. Irving Blifford and Junge initiated this investigation to determine the relative importance of various processes in modifying the aerosol populations. James Burgmeier was originally the programmer for the project, but later made contributions to the numerical implementation of the model, to improvement of numerical procedures, and to tests for assessing the accuracy and dependability of the computerized model. He also carried out stability studies to assure accuracy in long runs. Additionally, Blifford and Burgmeier have used the results and methods presented here as a starting point for more elaborate models. The research reported here was completed in summer 1972.

James W. Burgmeier

June 1974

CONTENTS

NOMENCLATURE

Symbol	Value	Units	Description or Definition
A	1.246	---	constant in Fuch's equation
a	2.0×10^{-5}	cm	constant in computing activated fraction
α	---	cm sec^{-1}	growth factor in differential equations, due to gas reactions
B	0.42	---	constant in Fuch's equation
b	0.31	---	average cloud cover
β	---	---	empirical factor in coagulation coefficient
C	0.87	---	constant in Fuch's equation
c	---	---	empirical factor in impaction efficiency
D	---	cm^2 sec^{-1}	factor in thermal coagulation
D_j	0.2	cm	average fiber diameter in impaction
E	5.0	---	constant in shear flow coagulation
ε	---	---	total efficiency in impaction
$\varepsilon_i, \varepsilon_{di}, \varepsilon_b$	---	---	efficiencies of collection in impaction
g	980.0	cm sec^{-2}	gravitational constant
$\overline{H}$	5.0×10^4	cm	troposphere or boundary layer height
$\overline{h}$	1000.0	cm	height of obstacles
h	1.5×10^5	cm	height of clouds

Symbol	Value	Units	Description or Definition
η	0.1	---	fraction of air filled with clouds
J	---	$cm^{-4}\ sec^{-1}$	coagulation integrals
K	---	$cm^{3}\ sec^{-1}$	coagulation coefficient
K_C	---	$cm^{3}\ sec^{-1}$	thermal coagulation coefficient
K_{SF}	---	$cm^{3}\ sec^{-1}$	shear flow coagulation coefficient
K_A	---	$cm^{3}\ sec^{-1}$	sedimentation coagulation coefficient
$\hat{K}$	---	$cm^{3}\ sec^{-1}$	coagulation coefficient with raindrops
k	1.805×10^{-18}	$gm\ cm^{2} sec^{-2} grad^{-1}$	Boltzmann's constant
κ	---	---	fraction of activated particles in clouds
L	1.0×10^{-6}	$cm^{3} H_2O\ cm^{-3}$ air	liquid water content of clouds
ℓ	6.0×10^{-6}	cm	mean free path of air molecules*
Λ_j	---	hr^{-1}	"rate constant" for process j.
λ	---	---	ratio of particle radius at 100% humidity to that at 50% (in clouds)
ΔM_d	---	gm	mass increase due to attachment of unactivated particles to activated ones
ΔM_f	---	gm	mass increase due to diffusiophoresis
ΔM_g	---	gm	mass increase due to oxidation of gases in clouds
ΔM_s	---	gm	mass increase due to interception of drops by other falling drops

Symbol	Value	Units	Description or Definition
ΔM_t	---	gm	$\Delta M_d + \Delta M_f + \Delta M_g + \Delta M_s$
m	---	---	number of discrete radii values in numerical quadrature ruler
μ	1.79×10^{-4}	gm cm^{-1} sec^{-1}	viscosity of air*
N(r,t)	---	cm^{-3}	number of particles per cubic cm of air with radius r at time t
n(r,t)	---	cm^{-4}	$\partial N/\partial r$
$n_1(r,t)$	---	cm^{-4}	aerosol fraction outside clouds
$n_2(r,t)$	---	cm^{-4}	activated aerosols inside clouds
$n_3(r,t)$	---	cm^{-4}	unactivated aerosols inside clouds
n_c	200.0	cm^{-3}	cloud drop concentration
$n_s(t)$	---	cm^{-4}	number of SO_2 particles at time t
ν	10.0	---	number of condensation-evaporation cycles
$\hat{\nu}$	0.14607	cm^2 sec^{-1}	kinematic viscosity of air*
p_h	1.9×10^{-6}	$cm^3 H_2O cm^{-2} sec^{-1}$	average rainfall rate
R	0.08	cm	radius of falling raindrops
r	---	cm	radius of aerosol particles
r_a	3.0×10^{-7}	cm	lower limit of particle size range
r_b	1.0×10^{-2}	cm	upper limit of particle size range
r_c	1.0×10^{-3}	cm	raindrop size
r_s	1.0×10^{-8}	cm	radius of SO_2 molecule
$\Delta r_1, \Delta r_1^*$	---	cm	radius increases of particles outside clouds
$\Delta r_2, \Delta r_2^*$	---	cm	radius increases of particles

Symbol	Value	Units	Description or Definition
			outside clouds
ρ_s	2.0	gm cm^{-3}	particle density
S	5000.0	cm	average path length of particle trajectory through vegetation
T	300.0	degree Kelvin	air temperature*
t	---	sec	time
τ	7200	sec	average life time of clouds
V(r)	---	sec^{-1}	$V(r)/\bar{H}$ = sedimentation velocity
w	300.0	cm sec^{-1}	horizontal wind velocity
Φ	2.0×10^{-19}	gm $cm^{-3} sec^{-1}$	production rate of SO_2
Φ*	1.9×10^{-19}	gm $cm^{-3} sec^{-1}$	production rate of organics
$\xi(r)$	---	$cm^3 H_2O cm^{-3}$	raindrop collection efficiency

* a function of altitude

1. Introduction

From observations carried out over the last two decades in polluted, and more recently in clean tropospheric air, it appears that atmospheric aerosols exhibit certain regular features which are more or less independent of the time or place of measurement. These features are not yet well understood, partly because the phenomena are complex and partly for lack of systematic studies. It is becoming increasingly obvious that a generalized picture which is based on the theoretical concepts of aerosol physics would be valuable in many scientific areas such as the global radiation, cloud physics, pollution, etc. It seems reasonable to base such studies on theoretical descriptions of the processes that change the distribution of particle size in the hope that these efforts may lead to an improved understanding of the experimental results. We wish to know how specific physical processes affect aerosols in the atmosphere, and in addition, we hope to gain sufficient insight into the problem to demonstrate how these individual processes combine to produce the observed size and number distributions.

In general, the size and number distribution of natural aerosols is determined by:

(1) Strength, location, and size distribution of the various natural and anthropogenic aerosol sources.

(2) Modification of the resulting aerosol size distribution by physical and chemical processes within the troposphere.

(3) Mixing due to transport.

(4) Natural processes that tend to remove aerosols (sinks).

It was pointed out recently that some of the basic features of the tropospheric aerosol size distribution may result from statistical effects brought about by random contributions from a large number of aerosol sources (Junge, 1969). However, the validity of this suggestion is difficult to demonstrate and will remain in question until it is understood to what extent processes (2), (3), and (4) are of importance within the troposphere and until additional experimental data are available.

In this paper we attempt to assess the importance of processes (2) and (4) by means of computer modeling techniques using models that are based on quantitative formulations of the processes involved. Our studies are an extension of earlier work begun several years ago by Junge (1964) and Junge and Abel (1965), who first attempted an investigation of this kind.

2. Tropospheric Aerosol Size Distributions

Our problem is to determine the rate at which, under atmospheric conditions, tropospheric aerosol distributions can change. Since the processes, in most cases, are not linear and depend on the shape of the entire size distribution, it is desirable to perform the computations with initial distributions which, although idealized for the purpose of the model calculations, are reasonably representative of tropospheric conditions. We have studied two typical tropospheric aerosol situations, a boundary layer model and a tropospheric model.

2.1 Boundary Layer Model (Urban Pollution)

This model postulates high aerosol concentrations within the planetary boundary layer of height $\overline{H}$ = 1000 m. Because horizontal transport

usually results in rapid reduction of the particle concentration by dilution, the computations are restricted to real-time intervals of two days. Since, in general, clouds are not present within the boundary layer, this model does not include any processes associated with clouds except rainout.

2.2 Tropospheric Model

This model postulates lower aerosol concentrations within the troposphere, which is assumed to have a height $\overline{H}$ = 10 km. Clean tropospheric air masses seem to be characterized by fairly uniform aerosols, which have average total particle concentrations of about 200-600 cm^{-3}. We estimate that about 80% of the troposphere is filled with this "background" aerosol and it is, therefore, of great importance for all global atmospheric phenomena. In this model, all of the processes associated with clouds are included and the time of integration is extended to ten days.

The above two cases do not adequately account for the entire range of tropospheric conditions but are sufficiently different to make it possible to illustrate the important effects.

2.3 Available Data for the Distribution

The shape of the distribution in polluted areas (Los Angeles) has been documented by Whitby (1971) and is similar to the distribution for the boundary layer model. Our knowledge of the shape of the background distribution is less satisfactory, but we have some information on the particle size range $0.1 \leq r \leq 3$ μm (Junge, Robinson, and Ludwig, 1969; Junge and Jaenicke, 1971; and Blifford and Ringer, 1969). Below and above these particle size limits little information is available.

Recent measurements have indicated that the distribution for particles with $10.0\ \mu m \leq r \leq 100\ \mu m$ may be much steeper than that for

particles 0.1 μm $\leq$ r $\leq$ 10.0 μm (Jaenicke, 1971). Too few measurements have been made to be certain of this point on the global scale and therefore we have for simplicity used the same slope (ν = -3) for the entire range 0.1 μm $\leq$ r $\leq$ 100 μm.

In the surface layer, over the ocean, we may expect to have the sea spray distribution superimposed on the above distribution. However, there is evidence that the sea spray component is restricted to the lowest 2 km in subtropical oceanic areas (Dinger, Howell, and Wojciechowski, 1970; and Gillette and Blifford, 1971). We suggest that the background aerosol of continental origin is rather uniformly mixed vertically over remote oceanic areas and that loss by washout and rainout in the lower layers is replaced from above by mixing. The sea spray components do not penetrate to higher layers over the ocean because washout is efficient and high humidity in the marine atmospheric boundary layer makes the condensation process an efficient scavenger of the soluble particles. Over the continents, due to convection originating in the dryer surface air, particles are transported to higher layers and are not as vigorously scavenged. Although this picture of the large-scale aerosol size distribution is still conjectural, since it is based upon very few data and is certainly a simplification, we feel that it is useful for the present studies.

A feature of the distribution which Junge and Jaenicke (1971) observed was the large number of extremely small particles, indicating the presence of a source of these particles. Our assumed curves on the other hand are parabolic with a maximum at 2 x 10^{-6} cm. We feel that they are reasonably good approximations to the cases considered in the present work.

Over the continents and in the polluted planetary boundary layer, we have assumed distributions like those of curve 1 of Fig. 1. Increasing distance from pollution centers, and horizontal and vertical dilution reduces the concentration. Above about 5 km over land and at a few thousand kilometers downwind from the continents we assume that the distribution has a form similar to that of curve 2 of Fig. 1.

3. Formulation of the Model for Computation

The aerosol model upon which our computations are based is intended to represent steady state conditions on a global scale. We assume a uniformly mixed troposphere in which a 1-cm^2 column of height $\overline{H}$ (tropopause height) is representative of average conditions. In this column the average fractional cloud cover b has height h, so that the average volume fraction filled by clouds is $\eta = \frac{bh}{\overline{H}}$. The clouds are assumed to have an average life time of τ hours before they evaporate or rain out, after which they immediately form again. We assume that each condensation nucleus goes through ν cycles of condensation and evaporation before it is removed from the air by rainout.

The following model, then, can be used to represent all of the aerosol changes which take place in the troposphere. We assume the original aerosol size distribution n(r,t) is composed of the three fractions $n_1(r)$, $n_2(r)$, and $n_3(r)$. The fraction of the total aerosol that is entirely in cloud-free air is

$$n_1(r,t) = (1-\eta)\, n(r,t)$$

while the volume fraction within the clouds is

$$n_2'(r,t) = \eta\, n(r,t)$$

where n_2' consists of a fraction $\kappa(r)$ containing the "activated" particles, i.e. are nuclei for condensation, and an "unactivated" fraction $[1 - \kappa(r)]$.

Therefore

$$n_2(r,t) = \eta\, \kappa(r)\, n(r,t)$$

and

$$n_3(r,t) = \eta[1 - \kappa(r)]\, n(r,t)$$

We assume that this division of the size distribution lasts for τ hours, during which time all three fractions are modified. The modifications are computed independently and at $t = \tau$ we assume that all clouds disappear, the three aerosol fractions mix completely and new clouds form. Thus the total distribution is given by

$$n(r,\tau) = n_1(r,\tau) + n_2(r,\tau) + n_3(r,\tau)$$

The process is then repeated--i.e., $n(r,\tau)$ is split into three portions, and modifications again occur separately until $t = 2\tau$, etc. Computations for any number of cycles can be performed by repetition of this scheme.

3.1 Rate Constants

A convenient way to compare all the processes involved in this

model is to use the "rate factors"

$$\Lambda_j(r,t) = \frac{3600}{t} \frac{\hat{n}(r,t) - \hat{n}(r,0)}{\hat{n}(r,t)}$$

where $\hat{n}(r,t)$, denotes one of the fractions n_1, n_2, or n_3. In order to make the comparisons valid, all processes governing n_1, for example, except the one under consideration are removed from the computations. Thus $\hat{n}$ denotes one of the three fractions, but with only one process involved. This technique enables us to compare the rate of each process in altering the distribution.

There will be a Λ associated with each process. The subscript placed on Λ will denote the process involved and coincides with the indexing in Fig. 2. For example, $j = 17$ for sedimentation in the calculation of n_1.

In some cases Λ_j changes with time and it was necessary to fix the time in order to compare all of the processes on the same basis. We have selected a real time of 2 hrs. The results of each computation are shown for $10^{-7} \leq r \leq 10^{-2}$ cm as log-log plots for positive and negative values of Λ_j between 10^{-5} and 10^{0} hr^{-1}. Rate constants slower than 10^{-5} hr^{-1}, even though they were computable, were judged to be insignificant on the scale of atmospheric effects and are not shown. In the curves, a positive value of Λ_j (upper portion of diagram) indicates that particles are being added and a negative value (lower portion) implies removal. Since both halves of the plots approach zero toward the center, a low value of Λ_j may in some instances cross

over to the adjacent half but have too small an absolute value to appear on either graph. Finally, we show the resulting changes in the size distribution function which results when all of the processes both within and outside of clouds are allowed to operate simultaneously.

3.2 The Meteorological Parameters η, τ, and ν

We do not have reliable average values for the three important meteorological parameters η, τ, and ν and consequently we attempt to estimate their probable range from general considerations. In middle latitudes we have good statistics on b and h for clouds at various levels. Up to 5 km (upper limit of aircraft observations) the average value of b seems to be about 31% and h must be larger than 5 km. If we assume $\overline{H}$ = 10 km we have

$$\eta = \frac{bh}{\overline{H}} = \frac{0.3 \times 5}{10} = 0.15$$

It may be argued that the fraction of the troposphere which is actively mixed is somewhat less than the tropopause height 10 km, but this is not very certain. However, in subtropical latitudes, for example, b and h are smaller and therefore the fraction of cloud-filled air will be smaller than 0.15. Thus the range of η values likely to occur in various climates is $0 \leq \eta \leq 0.2$, with 0.05 to 0.1 the most probable range for a global average.

We have some data on τ for convective clouds, where it is of the order of 0.5 to 1.0 hr. Considering the longer live times of layer clouds, we feel that $1 \leq \tau \leq 3$ hr may be the most likely range for a global average.

We require values of the quantity ν which are estimated from the following considerations: Since the average fraction of the air that is filled with clouds is η, each condensation nucleus should on the average be used for one condensation in $1/\eta$ cycles. The fraction of the total volume of a vertical column of 1 cm^2 and height $\bar{H}$ that is removed in $1/\eta$ cycles by the rainfall rate p_h(cm^3 H_2O cm^{-2} sec^{-1}) is

$$\frac{\tau p_h}{\eta \bar{H} L} = \frac{1}{\nu}$$

where τ is time for one condensation evaporation cycle and L is the liquid water content of clouds (cm^3 H_2O cm^{-3} air). Using the average values of the parameters $\eta = 0.1$, $L = 10^{-6}$, $\tau = 2$ hr, $p_h = 10^{-6}$, and $\bar{H} = 10^6$ cm, we find the order of magnitude of ν to be

$$\nu = \frac{\eta \bar{H} L}{\tau p_h} = 5$$

Although the condensation nuclei are removed by rainout, in view of the uncertainty of the average values for η, L, τ, and because perhaps one-half to one-third of the precipitation falling out of clouds does not reach the ground, the range of possible ν values may be as large as $1 < \nu < 30$.

3.3 The Distribution Function

If N is the number of particles with radius $\leq$ r per cubic centimeter, the size distribution is given by

$$n(r,t) = \frac{\partial N(r,t)}{\partial r} \; [cm^{-4}]$$

Since the range of size and concentration extends over many orders of magnitude, it is convenient to use logarithmic scales for plotting n and r and to relate the ordinate to the number density per unit of logarithmic radius, d(log r), the total number of particles between r and r + dr being equal to the area, d(log r) x $\frac{dN}{d(\log r)}$. This leads to the distribution

$$n^* (r,t) = \frac{\partial N}{\partial(\log r)} = (\ln 10) r \; n(r,t)$$

Although n was used in the computations, the results are plotted in terms of n*. Presently available data indicate that the maximum of n* is located in the radius interval 0.01 μm $\leq$ r $\leq$ 0.1 μm. For particle sizes less than 0.01 μm, n* must decrease for decreasing r. Above r = 0.1 μm, n* can be approximated by

$$n^* (r,t) = n^* (r_o,t) \left(\frac{r_o}{r}\right)^{-\nu^*}$$

where ν^* is approximately constant and generally has a value between 2 and 4. In the computations, the function log n*(r,0) was chosen to be a parabola for 0.003 μm $\leq$ r $\leq$ 0.1 μm, while for r > 0.1 μm, a straight line was used. The parabola has its maximum at 0.02 μm and the two portions of the curve are pieced together in such a way that log n*(r,0) and $\frac{d}{dr}$log n*(r,0) are continuous.

4. Processes of Aerosol Modification in the Troposphere

All of the modification processes which we have considered in our aerosol model are shown in outline form in Fig. 2. We will first discuss only those processes that affect the fraction $n_1 = (1-\eta)n$ of the aerosol which is outside of clouds. The fraction of the total aerosol inside of clouds (n_2 and n_3) is treated in subsequent sections. The physical basis for each portion of the computations will be described here separately in the order in which it is given in the outline. The numerical results are discussed in the same order in Section 8.

4.1 Particle Interactions (11, 12, 13)

The first processes that we consider are those involving interactions of particles with one another. As listed in Fig. 2, they are:

Thermal coagulation (Brownian motion);

Sedimentation coagulation (collection due to differences in fall rate); and

Shear-flow coagulation (collection by turbulent air motion).

All of these processes are treated conveniently by the same equation. The rate of change of the distribution function n_1 is given in this case by

$$\frac{\partial n_1(r,t)}{\partial t} = \int_{r_a}^{r/\sqrt[3]{2}} K(\sqrt[3]{r^3-\rho^3},\rho)\, n_1(\rho,t)\, n_1(\sqrt[3]{r^3-\rho^3},t)\, \frac{r^2}{(r^3-\rho^3)^{2/3}}\, d\rho$$

$$- n_1(r,t)\int_{r_a}^{r_b} K(r,\rho)\, n_1(\rho,t)\, d\rho \qquad (4.1.1)$$

where $r_a \leq r \leq r_b$. The first term on the right hand side of Eq. (4.1.1) represents the increase in number of particles of size r due to the addition of particles of equivalent volume formed when two particles of different sizes combine. This assumes that both the old and new particles are spherical which, of course, will be true only for coalescing liquid drops. Although this assumption is not generally valid for aerosols, it is a good approximation, especially at high humidity. The second term takes into account the loss of particles of size r.

Following Friedlander (1965) we can express the coagulation coefficient as the sum of three terms

$$K = K_c + K_s + K_{SH} \tag{4.1.2}$$

where K_c, K_s, and K_{SH} indicate thermal, sedimentation, and shear flow coagulation respectively.

From Fuchs (1964)

$$K_c = K_c(r,\rho) = 2[D(r) + D(\rho)](r + \rho)\ \beta(r,\rho) \tag{4.1.3}$$

where

$$D(r) = \frac{kT}{3\mu}\frac{1}{r}\left[1 + \frac{\ell}{r}\left(A + Be^{-Cr/\ell}\right)\right] \tag{4.1.4}$$

k is Boltzman's constant, T is temperature, and μ is viscosity. The expression within brackets contains the mean free path ℓ and the Cunningham slip correction which is necessary when the dimensions of the aerosol particles approach the mean free path of the air molecules.

The factor β is a semi-empirical expression which corrects for the fact that during collision small particles pass through a concentration discontinuity at the surface of larger particles. It is given by

$$\beta(r,\rho) = \left\{ \frac{r + \rho}{r + \rho + \delta_r} + \frac{\rho_s[D(r) + D(\rho)]}{3(r + \rho)G_r} \right\}^{-1}$$

where

$$G_r = \sqrt{\frac{1}{r^3} + \frac{1}{\rho^3}}$$

$$\delta_r = \sqrt{2[\chi^2(r) + \chi^2(\rho)]}$$

$$\chi(r) = \frac{1}{6r\ell_B(r)}\left\{ \left[2r + \ell_B(r) \right]^3 - \left[4r^2 + \ell_B^2(r) \right]^{3/2} \right\} - 2r$$

and

$$\ell_B(r) = \frac{1.637}{3\pi\mu}\sqrt{kT\rho_s r}\left[1 + \frac{\ell}{r}\left(A + Be^{-Cr/\ell} \right) \right]$$

We have used the approximate expressions as given by Friedlander (1965) for sedimentation coagulation

$$K_s(r,\rho) = \frac{\pi g \rho}{9\mu}\rho^2(r^2 - \rho^2), \quad r \geq \rho$$

$K_s(\rho,r) = K_s(r,\rho)$ and where g is the gravitational constant. For shear flow coagulation

$$K_{sh}(r,\rho) = 1.3 \frac{E}{\hat{\nu}} (r + \rho)^3$$

where E is a dimensionless constant $\simeq 5.0$ and $\hat{\nu}$ the kinematic viscosity (cm^2 sec^{-1}).

4.1.1 Thermal Coagulation (11)

Figure 3a shows the rate constant Λ_{11} as a function of particle radius for thermal coagulation alone. The relatively fast removal of particles of $r < 5 \times 10^{-6}$ μm is clearly seen. The smaller particles which disappear from the distribution reappear as larger particles, mainly in the region of 5×10^{-6} cm to 10^{-4} cm of the size spectrum. The effect of this process on the large particle portion of the distribution is negligible. For the tropospheric model in which the particle concentration is adjusted to a value of the concentration observed in experimental measurements in clean air, Λ_{11} corresponds to a lifetime of a few hours for the smallest particles, with a relatively slow buildup of particles in the region of 0.1 μm. When the concentration is increased by a factor of 10^4 (pollution model) the disappearance of small particles is extremely fast and there is a correspondingly large increase in the mid-range of the spectrum.

4.1.2 Sedimentation Coagulation (12)

For the troposphere model the effect of sedimentation coagulation is too small to appear on the graph. The computed values of Λ_{12} ranged from the order of -10^{-10} hr^{-1} for the smallest particles to about -10^{-6} hr^{-1} for the larger particles.

Although this process is also small in the boundary layer model the form of Λ_{12} can be seen in Fig. 3b. It seems reasonable to consider

this process to have a negligible effect even in high particulate concentrations.

4.1.3 Shear Flow Coagulation (13)

Shear flow coagulation is also a relatively small effect; the computed values of Λ_{13} ranged from -10^{-8} hr^{-1} to about $+10^{-8}$ hr^{-1} for the troposphere model. In the boundary layer model the computed values of Λ_{13} were also very small as shown in Fig. 3b. From the above results it appears that both shear flow and sedimentation coagulation are negligible in comparison with thermal coagulation.

4.2 Homogeneous Gas Reactions (14)

Photo-oxidation of SO_2 or other gas reactions results in the formation of very small particles with radii of the order of $r_s \simeq 5 \times 10^{-8}$ cm which is smaller than the lower limit of integration r_a. We assume that the attachment rate of these small particles to the aerosol can be treated by the coagulation equation. Since the diffusion coefficient $D(r_s) >> D(r_a)$ and also $r_a >> r_s$, the coagulation coefficient can be written as

$$K(r,r_s) \simeq 2D(r_s)r\beta(r,r_s) \qquad (4.2.1)$$

The attachment rate of these particles to the aerosol is therefore given by

$$\frac{dn_s(t)}{dt} = 2D(r_s)n_s(t) \int_{r_a}^{r_b} \rho\beta(\rho,r_s)n_1(\rho,t)\, d\rho \qquad (4.2.2)$$

where $n_s(t)$ is the number of SO_2 particles at time t. The number of these particles colliding with an aerosol particle of radius r in the time interval $[t, t + \Delta t]$ is

$$K(r,r_s)n_s(t)\Delta t = 2D(r_s)r\beta(r,r_s)n_s(t)\Delta t$$

Multiplying this by $4\pi\rho_s r_s^3/3$ gives the mass increase due to these collisions. Letting $r + \Delta r_1$ denote the radius of the increased particle, we have

$$\Delta r_1 = \frac{2}{3r}D(r_s)\beta(r,r_s)\Delta t\ n_s(t)r_s^3 \qquad (4.2.3)$$

The rate of production of the H_2SO_4 particles is

$$\Phi = \frac{4\pi\rho_s}{3}\ r_s^3\ \frac{dn_s}{dt}$$

Using (4.2.2) in this equation and the result in (4.2.3) gives

$$\Delta r_1 = \frac{\Phi\beta(r,r_s)\Delta t}{4\pi\rho_s r\int_{r_a}^{r_b}\rho\beta(\rho,r_s)n_1(\rho,t)\ d\rho} \qquad (4.2.4)$$

4.3 Heteorgeneous Gas Reactions (15)

Gas-particle reactions such as probably take place in the presence of organic vapor (e.g., terpenes) would result in a layer of material on the surface of the aerosol particle. If Φ^* denotes the production rate of this organic matter then from reasoning similar to that in the previous subsection we obtain

$$\Delta r_1^* = \Phi^* \Delta t / 4\pi\rho_s \int_{r_a}^{r_b} \rho^2 n_1(\rho,t) \, d\rho \qquad (4.3.1)$$

for the radius increase due to attachment of these particles.

4.3.1 Results of Computations

In the computations, homogeneous and heterogeneous gas-particle reactions are treated as though the entire mass of a gas for which the production rates Φ and Φ^* are known, becomes attached to all of the particles in the distribution. Figure 4a shows the computed values of Λ_{14} and Λ_{15} for homogeneous and heterogeneous gas reactions respectively, as a function of particle radius for production rates $\Phi = \Phi^* = 2 \times 10^{-19}$ gm cm^{-3}. It may be seen that the effect of these processes in adding mass to the aerosol is appreciably less than that of thermal coagulation for the smallest particles and becomes approximately the same for particles of $r < 10^{-4}$ cm. Although Λ_{14} and Λ_{15} diverge somewhat near $r = 10^{-4}$ cm, they are generally similar.

Figure 4b shows the rate constants Λ_{14} and Λ_{15} for homogeneous and heterogeneous gas reactions in the boundary layer model. In this case the particle concentration was a factor of 10^4 larger than in the

tropospheric model and the height of the layer was assumed to be 1 km. Although the assumed production rates Φ and Φ^* were larger by a factor of 10^2, the calculated rate constants are lower than for the tropospheric model. The relatively lower values of Λ_{14} and Λ_{15} compared to those for the entire troposphere probably are due to the assumption of a higher particle concentration in the boundary layer.

4.4 Washout (16)

The aerosol concentration outside of clouds will be reduced by washout below the clouds. The total number of raindrops in the column of cross-sectional area 1 cm^2 is given by

$$N_R = \frac{3\tau p_h}{4\pi R^3}$$

where R = average raindrop radius and p_h = average rainfall. Let h denote the height of the clouds. Then a single raindrop with collection efficiency $\xi(r)$ $(0 \leq \xi(r) \leq 1)$ sweeps out $\pi R^2 h\ \xi(r)\ n_1(r,t)$ aerosol particles and therefore in the volume hb the concentration $n_1(r)$ is reduced by

$$\frac{\Delta n_1(r,t)}{N_R} = - \frac{\pi R^2 \xi(r) n_1(r,t)}{b}$$

Therefore the number of particles below the clouds surviving the washout is

$$\left[\frac{bh}{(1 - \eta)H}\ n_1(r,t) \right] e^{-\sigma(r)}$$

where

$$\sigma(r) = \frac{3\tau p_h \xi(r)}{4bR}$$

Values of $\xi(r)$ are given in Table I.

In the volume $[(1 - \eta)\overline{H} - bh]$, i.e., the volume above the clouds, the concentration remains $n_1(r,t)$ while in the volume bh below the clouds the concentration decreases. After a time τ the average concentration in cloud-free air becomes

$$n_1(r,\tau) = \frac{[(1-\eta)\overline{H} - bh]\, n_1(r,\tau-0) + bh\, n_1(r,\tau-0)\, \exp(-\sigma(r))}{(1-\eta)\overline{H}}$$

$$= n_1(r,\tau-0)\, [1-\delta(1-e^{-\sigma(r)})]$$

where

$$\delta = \frac{bh}{(1-\eta)\overline{H}}$$

and where $n_1(r,\tau-0)$ denotes the distribution before washout began.

4.1.1 Results of Computations

That washout removal of particles is effective mainly for the larger particles is indicated by the values for washout efficiency in Table I. The rate constant for washout, Λ_{16}, (Fig. 5), shows that the process is effective only for particles larger than about 10^{-4} cm. However, for these particles rather rapid removal will take place.

4.5 Sedimentation (17)

The sedimentation rate V of particles of density ρ_s is given by Stoke's Law (corrected):

$$V(r) = \frac{2r^2 g\rho_s}{9\mu}\left[1 + A\frac{\ell}{r} + B\frac{\ell}{r}\exp(-Cr/\ell)\right]$$

Assuming that there is always sufficient mixing

$$\frac{\partial n(r,t)}{\partial t} = \frac{-V(r)n(r,t)}{\overline{H}}$$

and therefore

$$n(r,t) = n(r,0)\ e^{-V(r)t/\overline{H}}$$

4.5.1 Results of Computations

Figure 6 shows the sedimentation rate constants Λ_{17} as a function of particle radius. While particles with radii smaller than about 1.0 μm are not affected appreciably, removal of the larger particles is clearly quite rapid.

4.6 Attachment to Obstacles (18)

Particles may become attached to objects near the surface such as leaves of trees, grass, etc. This process has been considered by Toba (1965) and Tanaka (1966) in connection with sea salt distribution over land. Although they refer to the removal process as impaction, they do not actually calculate the effect directly. We use Eq. (4.6.1) to describe the attachment of particles to objects in the air stream:

$$\frac{\partial n_1(r,t)}{\partial t} = \frac{w\bar{h}}{S\bar{H}} \varepsilon(w,r) n_1(r,t) \qquad (4.6.1)$$

where w is the wind velocity, S the average path length of the particle trajectory within the layer, and $\varepsilon(w,r)$ is the efficiency of the attachment process. S is more-or-less equivalent to the visibility range through the obstacles; $\bar{h}$ is the average height of the obstacles (trees, etc.). Equation (4.6.1) is, of course, only an approximation to a very complex process.

By analogy with particle collection by fibers we assume the efficiency factor to be composed of three parts

$$\varepsilon(w,r) = \varepsilon_i + \varepsilon_{di} + \varepsilon_b$$

where ε_i, ε_{di}, and ε_b are the efficiencies of inertial impaction, direct interception and Brownian diffusion.

The inertial impaction efficiency $\varepsilon_i = f(\psi)$ is a function of the nondimensional impaction parameter ψ which is defined by the equation

$$\psi^{1/2} = 2r\left[\frac{cw\rho_s}{18\mu D_j}\right]^{1/2} \qquad (4.6.2)$$

where $c = 1 + \frac{\ell}{r}[A + B \exp(-Cr/\ell)]$, D_j is the average fiber diameter (leaves, grass, etc.), and ρ_s is the particle density.

Efficiency as a function of the impaction parameter has been determined experimentally by Ranz and Wong (1952) and is given in Table II for round, long fibers and spherical particles. We use their values,

which present a somewhat idealized picture of vegetation, with Eq. (4.6.2) to obtain the efficiency as a function of particle size, Particles that are large compared to the obstacle diameter may be attached due to direct interception and

$$\varepsilon_{di} = r_i/r_j$$

or simply the ratio of aerosol radius to fiber radius. For very small particles Brownian motion may play a part, but for the rather coarse filter system under consideration, we feel that the effect is negligible.

4.6.1 Results of Computations

It is evident that the process of attachment to obstacles is relatively efficient as shown by the rate constants Λ_{18} plotted in Fig. 7. It appears that this effect will override both sedimentation and washout as a means for clearing the atmosphere of large particles.

The rate constant for this process was calculated assuming that impaction and direct interception are the principal effects. Direct interception is inversely proportional to the size of the objects (leaves, etc.) in the air stream. Impaction, on the other hand, is more efficient on small fibers, for example, and for higher wind velocities. The latter is shown by the two curves of Fig. 7 which were computed for wind velocities of 300 cm sec^{-1} and 1000 cm sec^{-1}.

4.7 The equations for n_1

All of the above processes operate simultaneously to modify the aerosol concentration outside of clouds and the complete equation in finite difference form becomes

$$n_1(r,t+\Delta t) = \Delta t \left\{ \int_{r_a}^{r/\sqrt[3]{2}} K(\sqrt[3]{r^3-\rho^3},\rho) n_1(\sqrt[3]{r^3-\rho^3},t) n_1(\rho,t) \frac{r^2}{(r^3-\rho^3)^{2/3}} d\rho \right.$$

$$- n_1(r,t) \int_{r_a}^{r_b} K(r,\rho) n_1(\rho,t)\, d\rho \qquad (4.7.1)$$

$$\left. - \left[\frac{V(r)}{\bar{H}} + \frac{\overline{wh}}{S\bar{H}} \varepsilon(w,r) \right] n_1(r,t) \right\} + n_1(r - \Delta r,\ t)$$

where $\Delta r = \Delta r_1 + \Delta r_1^*$ and the argument $r - \Delta r$ represents the shift in n_1 due to particle growth in processes 14 and 15.

Using this finite difference form we can derive the integro-differential equation for n_1. Let $J[n_1(r,t)]$ denote the first two terms in the braces in the above equation. Then subtracting $n_1(r,t)$ from both sides, dividing by Δt, and letting $\Delta t \to 0$ yields

$$\frac{\partial n_1(r,t)}{\partial t} = J[n_1(r,t)] - \left[\frac{V(r)}{\bar{H}} + \frac{\overline{wh}}{S\bar{H}} \varepsilon(w,r) \right] n_1(r,t)$$

$$- \alpha_1(r,t) \frac{\partial n_1(r,t)}{\partial r} \qquad (4.7.2)$$

where

$$\alpha_1(r,t) = (\Delta r_1 + \Delta r_1^*)/\Delta t$$

(see Eqs. 4.2.4 and 4.3.1).

5. The Activated Aerosol Within Clouds

For computational purposes we treat the particles that have served as condensation nuclei or are "activated" (the fraction κ) separately from the "unactivated" particles. We assume that the average cloud contains 200 drops cm^{-3}. The larger particles in general are more efficient as nuclei and we therefore assume that a portion of the original model distribution consists of a fraction $\kappa(r)$ of activated particles and that the remainder of the particles in the cloud are not activated. We express this activated fraction as

$$\kappa(r) = e^{-(a/r)^2}$$

where a is chosen so that

$$\int_a^{r_b} n(r,0)\, dr = n_c$$

where n_c is the average number of cloud drops. The functional form e^{-x^2} is chosen as a matter of convenience to provide a sharp cutoff for $r < a$. Figure 8 shows how the starting function is modified when $\eta = 0.1$ and $n_c = 200$ to produce $n_2 = \eta\kappa(r)\, n$ and $n_3 = \eta(1-\kappa\ (r))\, n$. The activated fraction n_2 of the total aerosol distribution may be treated as though the processes act independently of those operating on the aerosols outside of clouds. The clouds are assumed to form instantaneously at time = 0 to last for time $t = \tau$ when the modification processes are repeated.

5.1 Coagulation of Cloud Droplets (21)

During the cycle τ, coagulation between cloud droplets results in a decrease in the number of activated particles. Since we assume that the droplets are of a uniform size, the coagulation coefficient is a constant, which we denote by $\hat{K}$. Consequently the equation governing this type of coagulation is

$$\frac{\partial n_2(r,t)}{\partial t} = \hat{K} \int_{r_a}^{r/\sqrt[3]{2}} n_2(\sqrt[3]{r^3 - \rho^3}, t) n_2(\rho,t) \frac{r^2}{(r^3 - \rho^3)^{2/3}} \, d\rho$$

$$- \hat{K} \, n_2(r,t) \int_{r_a}^{r_b} n_2(\rho,t) \, d\rho$$

Coagulation of cloud droplets is due not only to Brownian motion, but predominantly to turbulence, and therefore no data are available for $\hat{K}$. Our estimate of a value for $\hat{K}$ is based on the assumption that during a cycle τ, the concentration of cloud droplets decreases by a factor of 2 or 3. We chose

$$\hat{K} = \frac{2}{\tau n_c}$$

where n_c is the cloud droplet concentration.

5.1.1 Results of Computations

The rate constant Λ_{21} for particle size change resulting from coagulation of the cloud droplets within a cloud is shown in Fig. 9 as a function of particle size. The form of the function is similar

to that for thermal coagulation but the portion of the particle size spectrum affected is quite different. Of course, the small particles are not involved because it is assumed that only large particles serve as condensation nuclei.

5.2 Particle Growth at High Humidity (40)

The unactivated particles are in an environment of high humidity which results in an increase in radius. In the case of the activated particles this affects the processes of thermal coagulation of particles with cloud droplets and sedimentation coagulation with cloud droplets. Hence we discuss this humidity growth here rather than in the sections devoted to n_3. Particle growth is dependent upon particle size and on the type of aerosol (e.g., continental, maritime). However, the measurements of Winkler (1970) indicate that the ratio

$$\lambda = \frac{r_{100\%}}{r_{50\%}}$$

is nearly constant, $\lambda \simeq 1.7$.

In our model we assume there are $n_3(r,t)$ particles of radius r before humidity growth. Each particle grows to a radius of λr and after the growth there are $n_3(r,t)$ particles of radius λr, or $n_3(r/\lambda,t)$ particles of radius r. We assume that the clouds form instantaneously and that the increase in radius of each unactivated particle is also instantaneous. Consequently, in all calculations involving n_3, we must use the "shifted" values $n_3(r/\lambda,t)$. At time $t = \tau$ (and multiples thereof) the clouds are assumed to disappear, resulting in a shift in the opposite direction

from growth or

$$n_3(r,\tau) \rightarrow n_3(\lambda r,\tau)$$

Attachment of unactivated particles to cloud drops, oxidation of SO_2 and other gases, collection by falling drops, and diffusiophoresis, respectively, result in growth in particle mass by an amount

$$\Delta M_t = \Delta M_d + \Delta M_g + \Delta M_f + \Delta M_s$$

where: ΔM_d = mass increase due to attachment of unactivated particles;

ΔM_g = mass increase due to oxidation of SO_2 or other gases within cloud drops

ΔM_f = mass increase due to diffusiophoresis; and

ΔM_s = mass increase due to interception of drops by other falling drops.

The result of these mass increases is an increase in radius by an amount Δr_2:

$$\frac{r + \Delta r_2}{r} = \left[\frac{\frac{4\pi\rho_s}{3} r^3 + \Delta M_t}{\frac{4\pi\rho_s}{3} r^3} \right]^{1/3}$$

or

$$\Delta r_2 = r \left\{ \left[1 + \frac{3\Delta M_t}{4\pi\rho_s r^3} \right]^{1/3} - 1 \right\}$$

5.3 Thermal Coagulation of Particles with Cloud Droplets (22)

We assume that cloud drops are of uniform size $r_c = 10$ μm and are much larger than the unactivated particles. The number of unactivated particles that attach to each cloud droplet in a time interval $[t, t + \Delta t]$ is

$$\Delta t \int_{r_a}^{r_b} K(r_c,\rho) n_3(\rho,t)\, d\rho$$

The mass increase is

$$\Delta M_d = \frac{4\pi\rho_s}{3} \Delta t \int_{r_a}^{r_b} \rho^3 K(r_c,\rho) n_3(\rho,t)\, d\rho$$

Since $n_3(\rho,t)$ is very small for $\rho < a$ and since $a \ll r_c$, we can simplify $K(\rho,r_c)$ to

$$K(\rho,r_c) = \frac{2kT}{3\mu} D(\rho) r_c$$

and thus

$$\Delta M_d = \frac{8\pi kT\rho_s r_c \Delta t}{9\mu} \int_{r_a}^{r_b} \rho^2 \left[1 + \frac{\ell}{\rho}(A + Be^{-C\rho/\ell})\right] n_3(\rho,t)\, d\rho$$

where the form for $D(\rho)$ given in Eq. (4.1.4) has been used.

5.3.1 Results of Computations

Figure 10 shows the calculated rate constant for thermal

coagulation of particles with cloud droplets, Λ_{22}. The effect is small and is appreciable only for particles of $r \simeq 10^{-5}$ m. The computations include the correction for growth of the unactivated particles in high humidity.

5.4 Sedimentation Coagulation of Particles with Cloud Droplets (23)

As the cloud droplets fall, unactivated particles become attached to them. The number of unactivated particles attaching to each cloud drop per unit time is

$$\int_{r_a}^{r_b} K_s(\rho, r_c) n_3(\rho, t)\, d\rho$$

where n_3 reflects the growth due to humidity discussed in Sec. 5.2. As a consequence, the increase in mass of the activated particles in a time $[t, t + \Delta t]$ is

$$\Delta M_s = \frac{4\pi\rho_s \Delta t}{3} \int_{r_a}^{r_b} \rho^3 K_s(\rho, r_c) n_3(\rho, t)\, d\rho$$

The function K_s is defined in Sec. 4.1.

5.4.1 Results of Computations

The rate constant for sedimentation coagulation of particles with cloud droplets Λ_{23}, is shown in Fig. 11. It may be seen that it is quite similar in form to Λ_{22}, but a little smaller in magnitude. The computations include the correction for particle growth at high humidity.

5.5 Diffusiophoresis (24)

When cloud drops condense, the process called diffusiophoresis results in an increase in particle radius. Goldsmith, Delafield, and Cox (1963) gives the fractional increase in size as 4.5×10^{-6}, independent of size. The mass increase is given by

$$\Delta M_f = 6\pi \times 10^{-6} \int_{r_a}^{r_b} \rho^3 n_3(\rho,t)\, d\rho$$

5.5.1 Results of Computations

The computed values for Λ_{24}, the rate constant for the diffusiophoretic effect, were generally less than 10^{-7} hr^{-1}. The values were too small to be plotted on the scale chosen and can be considered to be negligible.

5.6 Heterogeneous Gas Reaction (25)

The mass increase due to this process is

$$\Delta M_g = \frac{1.6 \times 10^{-6}}{\nu} r_c^3$$

and is applied only once in each cycle τ.

5.6.1 Results of Computations

It is clear from Fig. 12 that Λ_{25}, the rate constant for heterogeneous gas reactions with cloud droplets, is similar to that for the other processes that add mass to the activated particles.

5.7 Rainout (26)

The fraction of the air within clouds in which rain occurs in

each cycle is $1/\nu$. Therefore, the fraction n_2 is reduced by a factor $\nu-1/\nu$ at the end of each cycle of condensation.

5.7.1 Results of Computations

Figure 13 shows the computed values of Λ_{26}, the rate constant for rainout. This process is less efficient than washout by a factor of 10.

5.8 The Equations for n_2

Combining the above processes into one equation leads to

$$n_2(r,t+\Delta t) = \Delta t \left\{ \int_{r_a}^{r/\sqrt[3]{2}} \hat{K}\, n_2(\sqrt[3]{r^3-\rho^3},t)\, n_2(\rho,t)\, \frac{r^2}{(r^3-\rho^3)^{2/3}}\, d\rho - n_2(r,t) \int_{r_a}^{r_b} \hat{K}\, n_2(\rho,t)\, d\rho \right\} + n_2\left(r-\Delta r_2, t\right)$$

This equation is employed for the calculation of n_2 when $i\tau < t+\Delta t \leq (i+1)\tau$, and i is an integer. As mentioned earlier, when the time t is a multiple of τ, mixing occurs, resulting in a new n_2.

As with n_1, the integro-differential equation for n_2 can be derived from this finite difference form. It is

$$\frac{\partial n_2(r,t)}{\partial t} = \hat{K} \int_{r_a}^{r/\sqrt[3]{2}} n_2(\sqrt[3]{r^3-\rho^3},t)\, n_2(\rho,t)\, \frac{r^2}{(r^3-\rho^3)^{2/3}}\, d\rho - \hat{K}\, n_2(r,t) \int_{r_a}^{r_b} n_2(\rho,t)\, d\rho - \alpha_2(r,t)\, \frac{n_2(r,t)}{\partial r}$$

where $\alpha_2(r,t) = \Delta r_2/\Delta t$

and where

$$\Delta r_2 = r\left\{\left[\ 1 + \frac{3(\Delta M_d + \Delta M_s)}{4\pi\rho_s r^3}\ \right]^{1/3} - 1\right\}$$

The initial condition is

$$n_2(r,0) = \eta\kappa(r-\hat{\delta})n(r-\hat{\delta},0)$$

where

$$\hat{\delta} = r\left\{\left[\ 1 + \frac{3(\Delta M_g + \Delta M_f)}{4\pi\rho_s r^3}\ \right]^{1/3} - 1\right\}$$

6. The Unactivated Aerosol Within Clouds

The remainder of the particles within the clouds are in the unactivated fraction $n_3(r,t)$. Three processes affect the distribution $n_3(r,t)$ as shown in Fig. 2: thermal coagulation of these particles with themselves, thermal coagulation with cloud droplets, and heteorgeneous gas reactions.

6.1 Thermal Coagulation (31)

The modifications of $n_3(r,t)$ caused by thermal coagulation are the same as for n_1, as given by Eq. (4.1.1), with n_1 replaced by n_3. Consequently, we will not write the equation for this process.

6.1.1 Results of Computations

Figure 14 shows the rate constant Λ_{31}, for thermal coagulation of the unactivated particles within clouds. The form of curve is similar to that of Fig. 3, as is to be expected. However, the

process is considerably less efficient in changing the size distribution.

6.2 Coagulation with Cloud Droplets (32)

As in Sec. 5.2, the unactivated particles become attached to cloud droplets, resulting in a decrease in the number of unactivated particles.

The number of unactivated particles of radius r that attach to cloud droplets at time t per unit time is

$$K(r_c,r)\ n_c\ n_3\ (r,t)$$

and the rate of change of n_3 particles due to this process is

$$\frac{\partial n_3(r,t)}{\partial t} = -\ K(r_c,r)\ n_c\ n_3(r,t)$$

Since $r_c >> r$ in this case, $K(r_c,r)$ simplifies to

$$K(r_c,r) = 2D(r)r_c$$

Using the expression (4.1.4) for D, we obtain

$$\frac{\partial n_3(r,t)}{\partial t} = -\ q(r)\ n_3(r,t)$$

where

$$q(r) = \frac{2r_c n_c}{r}\left[1 + \frac{\ell}{r}(A + be^{-Cr/\ell})\right]$$

Consequently, we have

$$n_3(r,\ t + \Delta t) = n_3(r,t)e^{-q(r)\Delta t}$$

as the number of unactivated particles at time $t + \Delta t$, considering only attachment to cloud droplets by thermal coagulation.

In addition to thermal coagulation there is attachment of particles by sedimentation coagulation, as discussed in Sec. 5.4. The number of unactivated particles of radius r which attach to cloud droplets per unit time through sedimentation coagulation is

$$K_s(r,r_c)\ n_c\ n_3\ (r,t)$$

resulting in

$$\frac{\partial n_3(r,t)}{\partial t} = -\ K_s(r,r_c)\ n_c\ n_3(r,t)$$

Combining this with the loss due to thermal coagulation with cloud droplets, we obtain

$$n_3(r,\ t + \Delta t) = n_3(r,t)e^{-q^*(r)\Delta t}$$

as the number of unactivated particles at time $t + \Delta t$, when only coagulation is considered. The function q^* is given by

$$q^*(r) = q(r) + K_s(r,r_c)n_c$$

6.2.2 Results of Computations

The rate constant for Λ_{32}, coagulation of unactivated particles within clouds with the cloud droplets, is shown in Fig. 15. It may be seen that this effect is quite strong for the smallest particles and negligible for particles of $r < 10^{-4}$ cm.

6.3.1 Heterogeneous Gas Reactions (33)

This process results in a growth of all particles by

$$\Delta r_2^* = \Delta t \ \Phi^*/4\pi\rho_s \int_{r_a}^{r_b} \rho^2 \ n_3(\rho,t) \ d\rho$$

as in the case of Δr_1^* for n_1 (Eq. 4.3.1).

6.3.2 Results of Computations

From the plot of Λ_{33} in Fig. 16, the rate constant for heterogeneous gas reactions with the unactivated particles within clouds is similar to that for Λ_{15}, shown in Fig. 4. In this case the large particle effect is less, probably because of the reduced number of large particles.

6.4 The Equations for n_3

Combining the three processes discussed above leads to the finite difference equation for n_3,

$$n_3(r,t+\Delta t) = \Delta t \left\{ \int_{r_a}^{r/\sqrt[3]{2}} K(\sqrt[3]{r^3-\rho^3},\rho) n_3(\sqrt[3]{r^3-\rho^3},t) n_3(\rho,t) \frac{r^2}{(r^3-\rho^3)^{2/3}} d\rho \right.$$

$$- n_3(r,t) \int_{r_a}^{r_b} K(r,\rho)\, n_3(\rho,t)\, d\rho \Bigg\}$$

$$+ n_3\left(r - \Delta r_2^*, t \right) e^{-q^*(r)\Delta t}$$

and

$$n_3(r,0) = u(r/\lambda)$$

where

$$u(\rho) = \eta[1 - \kappa(\rho)]\, n(\rho,0)$$

The integro-differential equation for n_3 is

$$\frac{\partial n_3(r,t)}{\partial t} = J[n_3(r,t)] - q^*(r) n_3(r,t) - \alpha_3(t) \frac{\partial n_3(r,t)}{\partial r}$$

where

$$\alpha_3(t) = \frac{\Delta r_2^*}{\Delta t}$$

(see Eq. 6.3.1).

7.0 Combined Effect of All Processes Acting Simultaneously

In order to show the general form of the change in the distribution function with time, we have adopted standard values of η, ν, and τ.

The results of computations using these values when all processes are allowed to operate are shown in Fig. 17 for times up to two days. There is a relatively fast and large reduction in particles of $r < 10^{-6}$ cm until at 12 hr the number of particles of this size has decreased by about three orders of magnitude. At 48 hr, the number of particles of $r < 5 \times 10^{-6}$ cm is negligible. The relative decrease of large particles is not as severe, although it appears that by 48 hr the number of particles of $r < 5 \times 10^{-4}$ cm has also been reduced to a negligibly small value.

7.1 Effects of the Parameter ν

The parameters η, ν, and τ are not very well known and therefore, it is of interest to see what effect variations of these quantities over a range of values that seems appropriate has on changes in the form of the distribution function with time. Figure 18 shows the results of computations with $\eta = 0.1$, $\tau = 7200$ sec, and ν, the number of condensation-evaporation cycles, allowed to take values from 1 to 30 for periods of up to 48 hr. It appears that the computation is not very sensitive to large values of ν. The tendency for an increase in the number of condensation cycles without rain to maintain a higher concentration of small and mid-range particles can be seen by comparing the 48-hr curves.

7.2 Effect of the parameter η

Figure 19 shows how the size distribution is affected when η, the fraction of aerosol outside of clouds, is varied while ν and τ have the fixed values of 5.0 and 7200 sec respectively. It may be seen that the relative reduction in the number of particles in the small particle region of the spectrum is greater than in the large particle

region. The computations indicate little change in the size distribution for values of $\eta = 0.1$, and $\eta = 0.2$. The overall effect for the range of η used was not vastly different than for the range of ν used in the previous computations.

7.3 Effect of the Parameter τ

Computations using $\eta = 0.1$, $\nu = 5.0$ while allowing τ (the average rain period) to vary, do not generally result in very different size distributions from those of the previous examples as seen in Fig. 20. The effect is seen to be principally in the small particle portion of the spectrum. After 48 hr, the reduction of the particle range $r < 10^{-5}$ cm is appreciably greater for a 1-hr rain cycle than for a 3-hr cycle. It appears that there will be very little difference in the particle spectrum for $r < 10^{-4}$ cm for this range of τ values.

8.0 Conclusions

In general, the change in the size distribution function with time exhibits some distinct and readily explainable features. There is a relatively rapid reduction with time in the number of the smallest particles due to coagulation. Sedimentation and attachment reduce the number of large particles, but at a lesser rate. In the first few hours, there is a tendency for the mass lost by the small particles to be transferred into the 0.1-μm size range. However, after several days, only particles of $0.1\ \mu m \leq r \leq 1.0\ \mu m$ remain.

It appears that variations in the rainout time τ, the number of condensation/evaporation cycles ν, and in the fraction of the aerosol outside of clouds η, have individually quite similar effects. Until better values of these parameters become available, it is probably not

worthwhile to select specific values. Of the above parameters, the use of small values of ν resulted in the most significant effect.

The computations in which the rates of each of the processes assumed for the model were determined separately are instructive in showing the relative importance of each. The most effective contribution to the rapid decrease of particles of $r < 10^{-5}$ cm is by coagulation. Sedimentation coagulation, shear flow coagulation, and particle/chemical reactions do not seem to be very effective in changing the form of the distribution. Sedimentation and washout are moderately important but only for $r < 10^{-4}$ cm. Attachment to obstacles in the air stream is suprisingly strong, but only for $r > 10^{-4}$ cm.

Processes that have to do only with the activated particles within clouds (coagulation of cloud drops, coagulation of particles with cloud drops and gas reactions), seem relatively ineffective in changing the size distribution. Even rainout, which has the largest rate constant ($r > 10^{-4}$ cm), seems not to be important. Rate constants for the unactivated particles within clouds indicate a rather rapid reduction of particles of $r < 10^{-5}$ cm by thermal coagulation with cloud drops. The other processes that we have assumed to take place within clouds seem to be less effective.

Unfortunately, very few experimental data that can be assumed to be reasonably independent of transport phenomena are available for comparison with the computed values. The data of Blifford (1970) indicate that both the smallest and the largest particles decrease with altitude. This is in accordance with the present results since older aerosols are expected to be present at the higher altitudes. Recent results of

Junge and Jaenicke (1971) indicate that over the Atlantic Ocean, far from land, the number does not decrease down to the smallest sizes measured ($r \simeq 10^{-7}$ cm). Since our computations indicate a rather rapid reduction in particles of this size, a maritime source capable of generating the smallest particles seems likely.

Table I

Removal Efficiency of Raindrops of 0.08 cm Radius (Mason 1957)

Particle Radius ($\times 10^{-4}$ cm)	Efficiency (r)
1	0.00
2	0.16
3	0.40
4	0.53
6	0.73
8	0.83
10	0.90

Table II

Experimental Impaction Efficiencies of Cylindrical Collectors (Ranz and Wong, 1952)

Impaction Parameter ($\psi^{\frac{1}{2}}$)	Efficiency
0.5	0.18
1.0	0.41
1.5	0.60
2.0	0.72

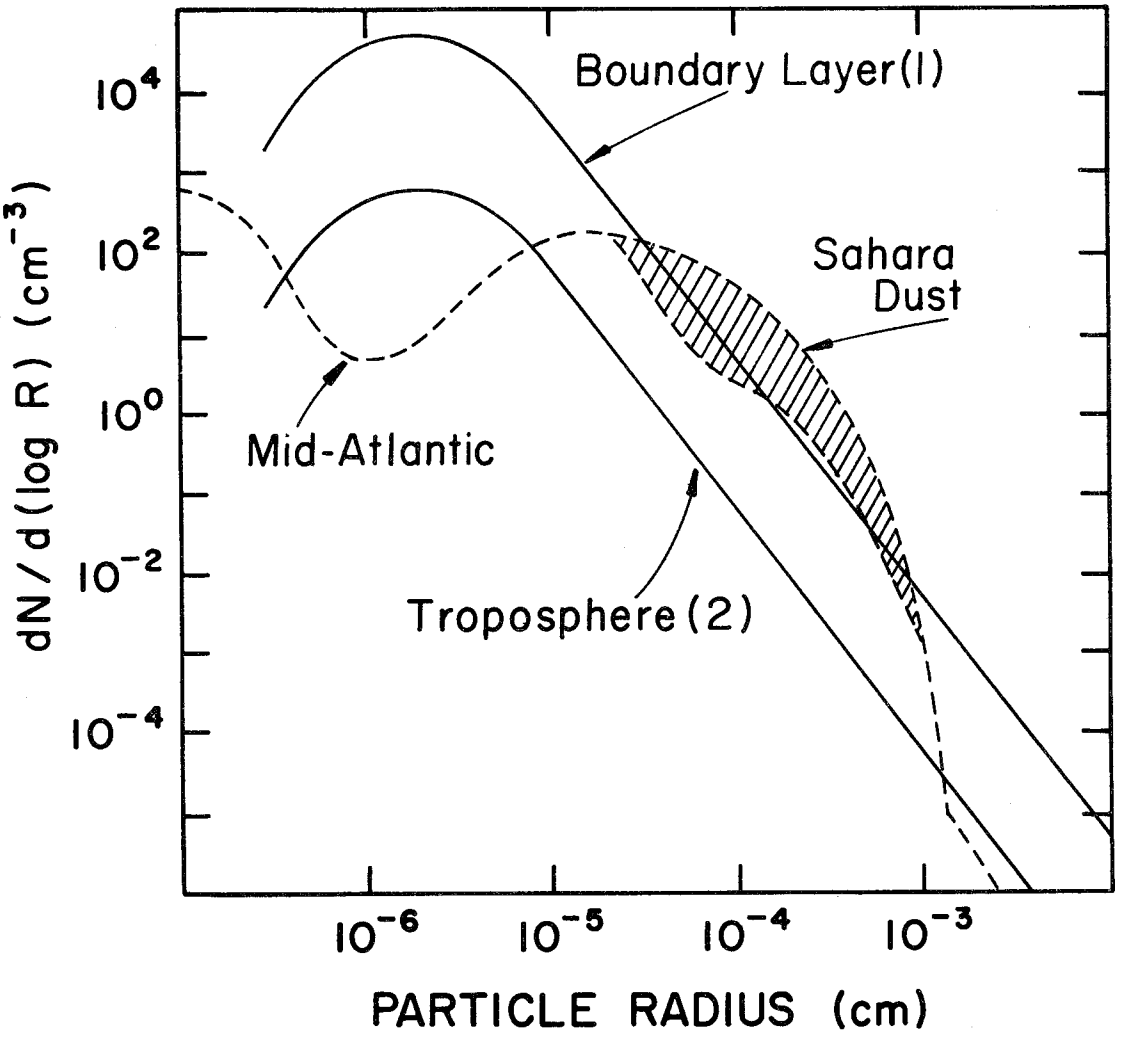

Fig. 1 Experimental size and number distribution and assumed distributions used in calculations

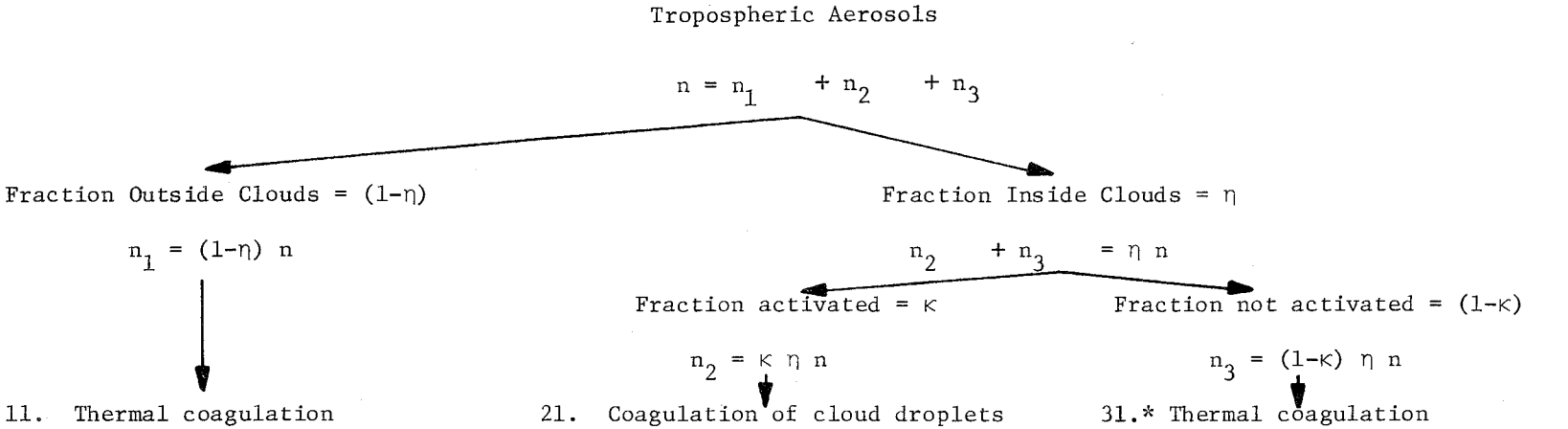

* Corrected for particle growth at high humidity

Fig. 2 Processes considered in computations

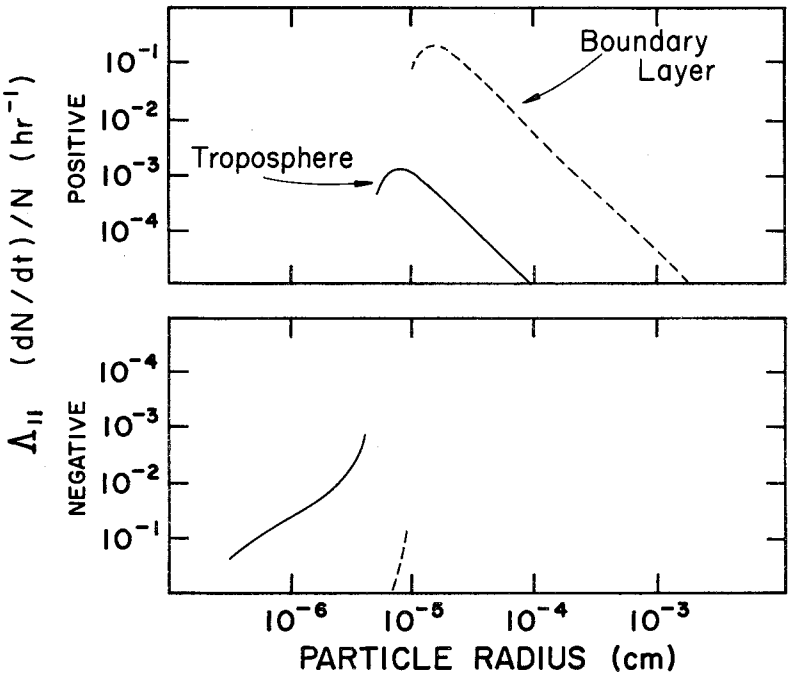

Fig. 3a Thermal coagulation of $n_1(r)$ particles

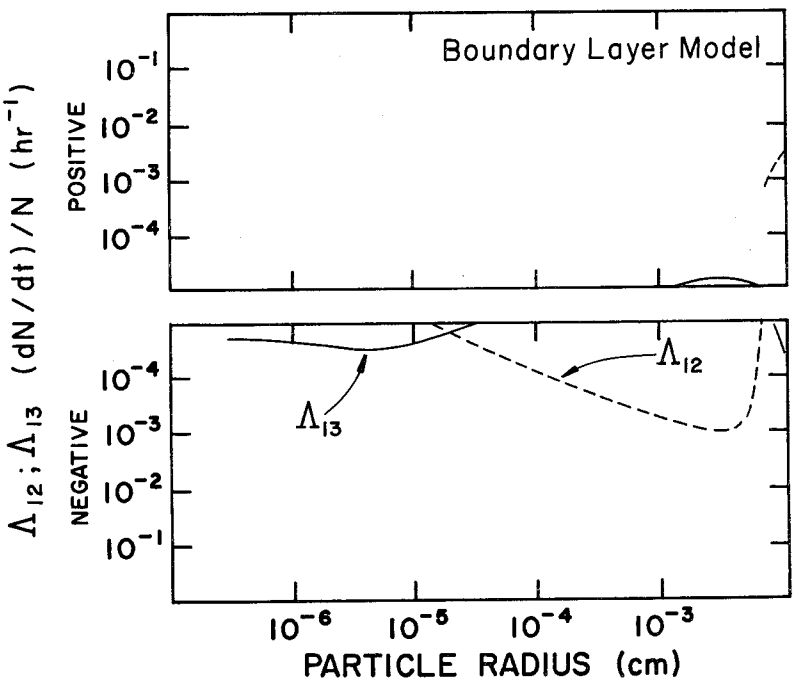

Fig. 3b Shear flow and sedimentation coagulation of $n_1(r)$ particles

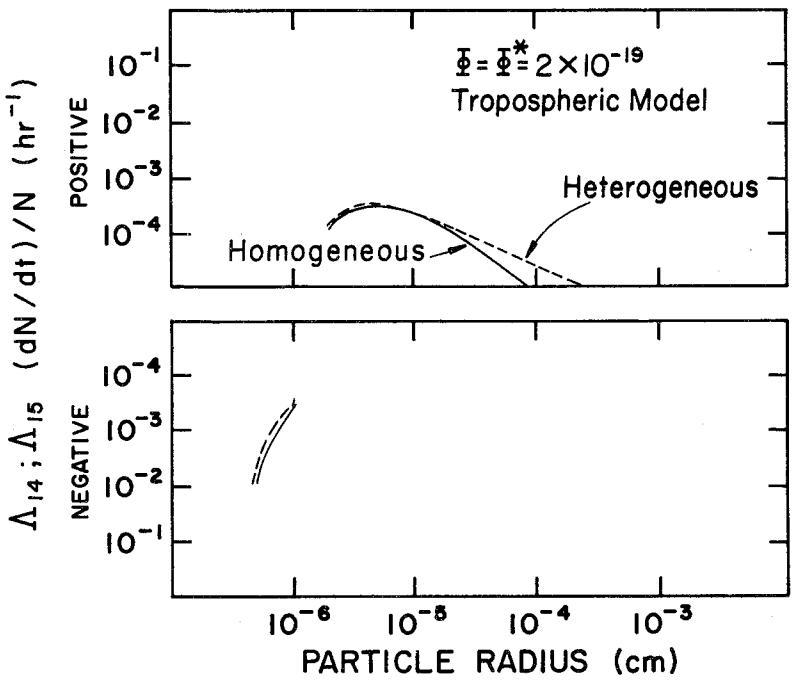

Fig. 4a Homogeneous and heterogeneous gas reactions, troposphere model, $n_1(r)$ particles

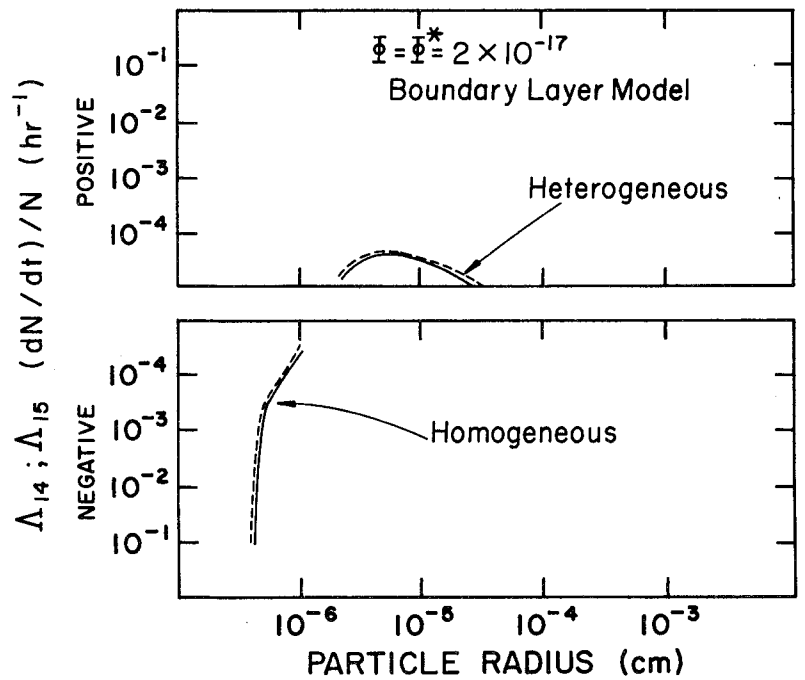

Fig. 4b Homogeneous and heterogeneous gas reactions, boundary layer model, $n_1(r)$ particles

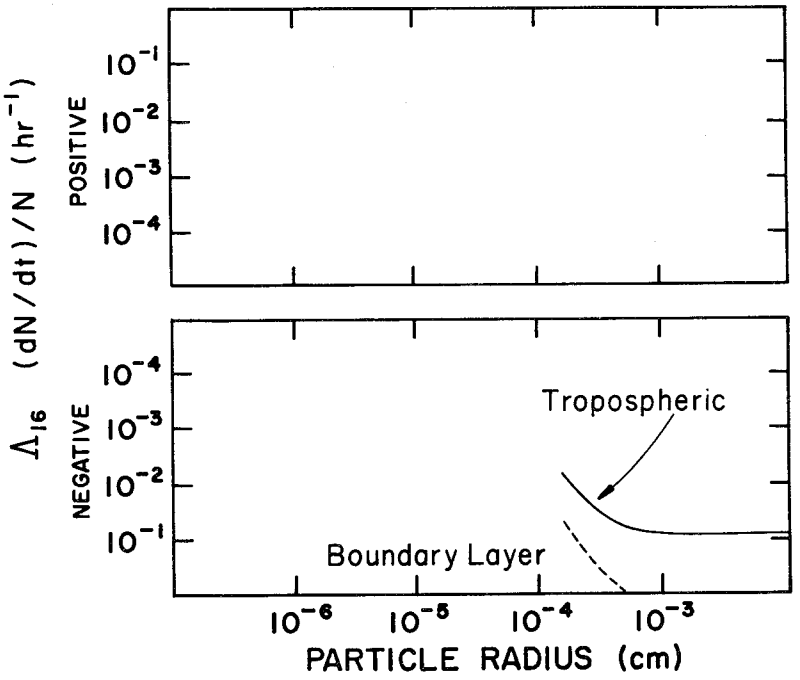

Fig. 5 Washout of $n_1(r)$ particles

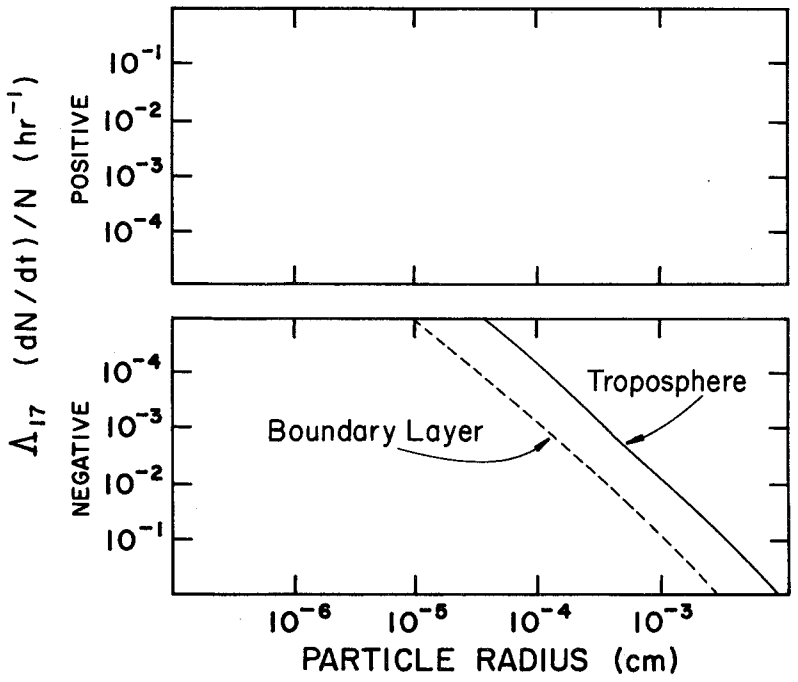

Fig. 6 Sedimentation of $n_1(r)$ particles

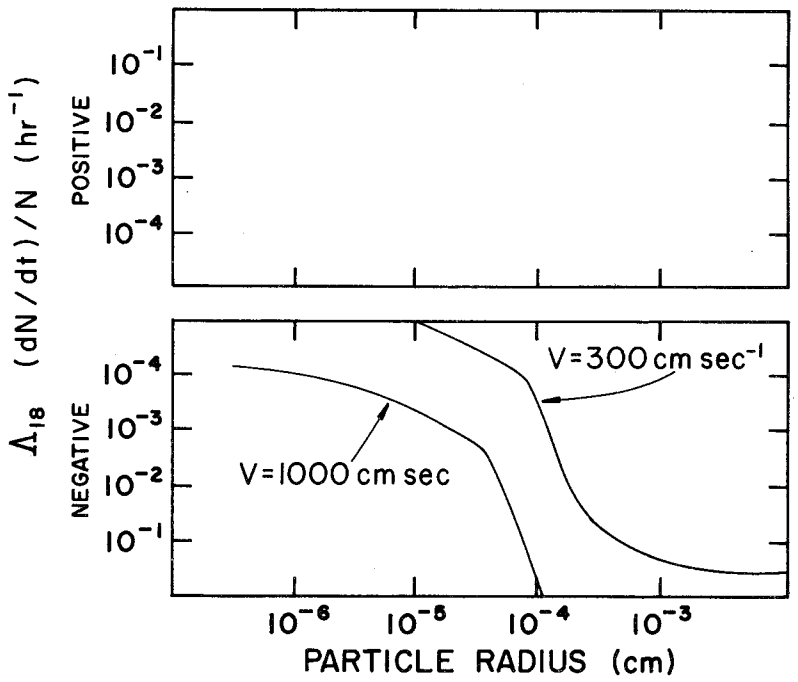

Fig. 7 Attachment of $n_1(4)$ particles

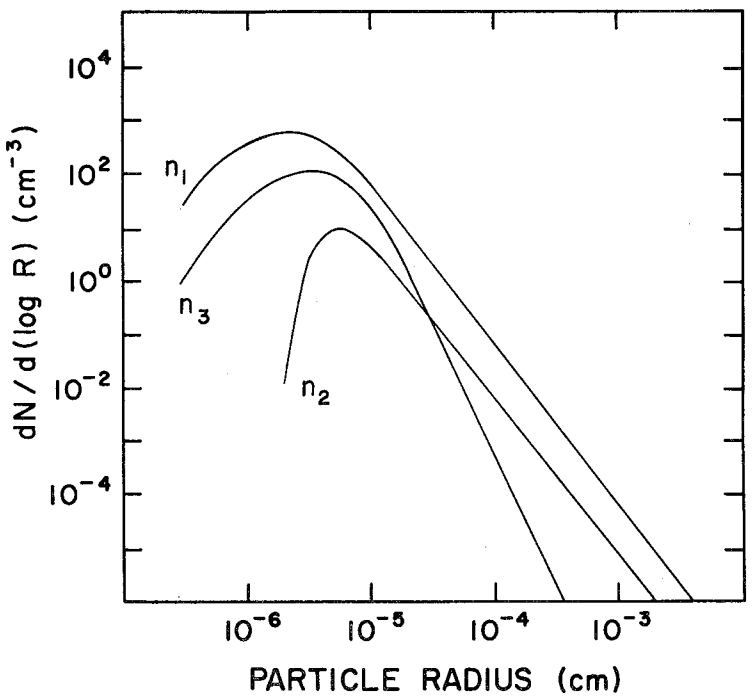

Fig. 8 Fractions of total atmospheric aerosol considered in model (initial distributions)

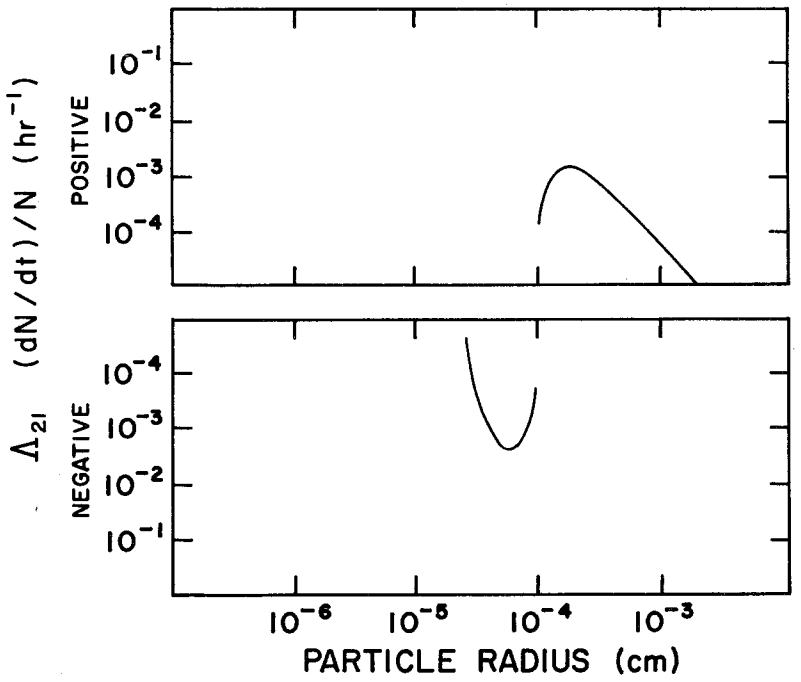

Fig. 9 Coagulation of cloud droplets, $n_2(r)$ particles

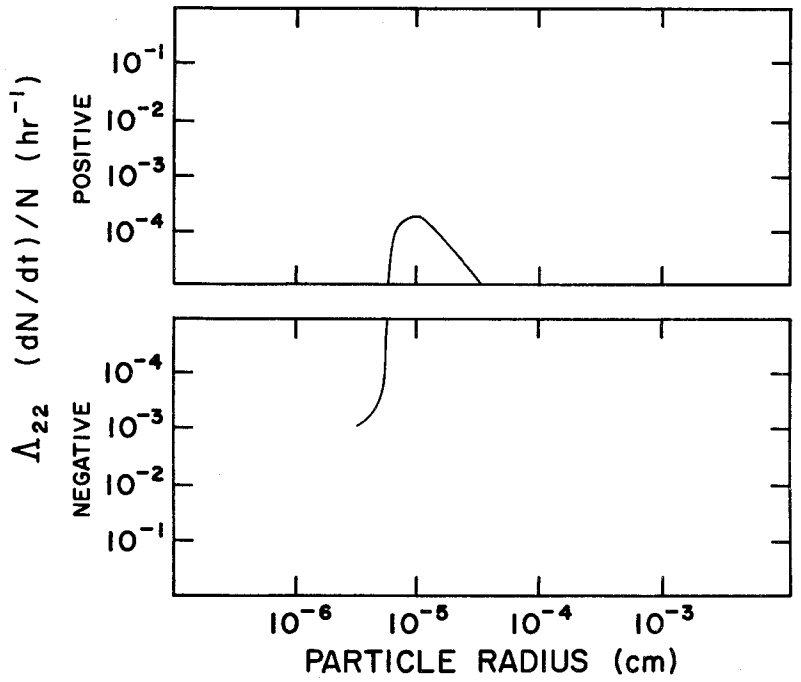

Fig. 10 Thermal coagulation of $n_2(r)$ particles with cloud droplets

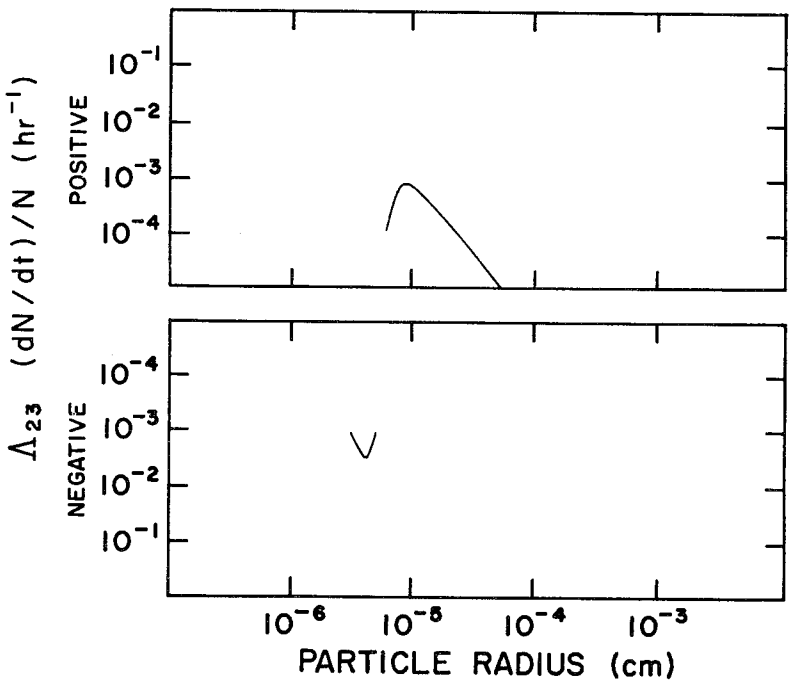

Fig. 11 Sedimentation coagulation of particles with cloud droplets, $n_2(r)$ particles

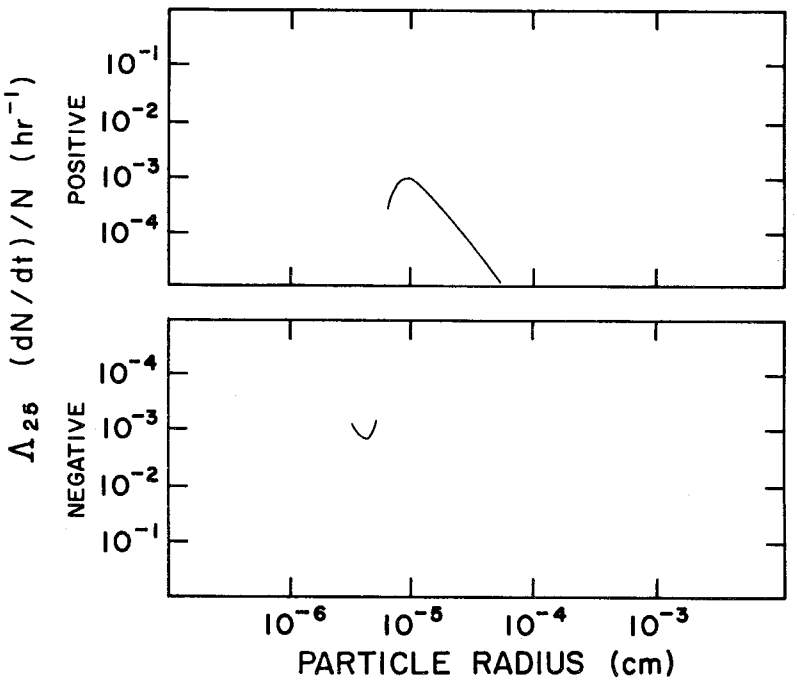

Fig. 12 Heterogeneous gas reactions, $n_2(r)$ particles

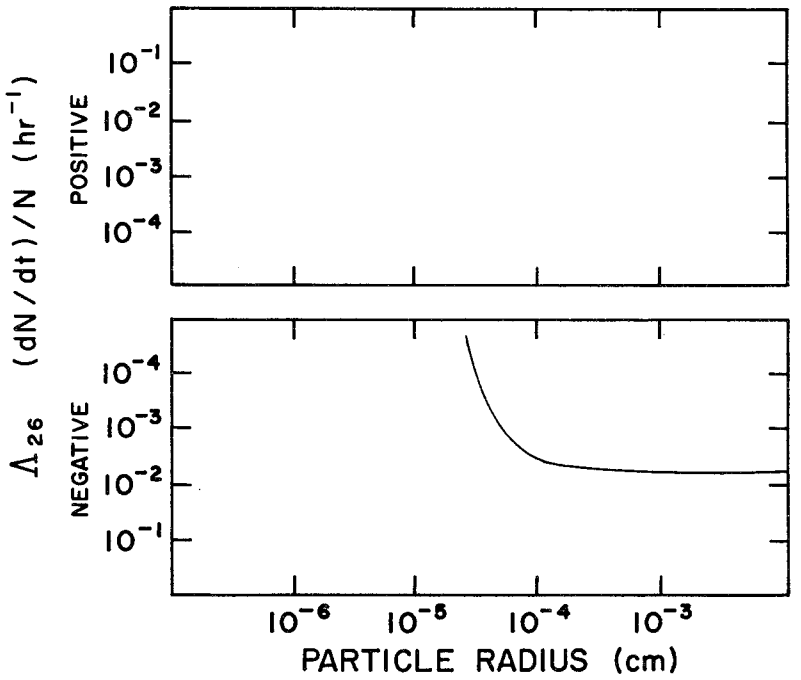

Fig. 13 Rainout of $n_2(r)$ particles

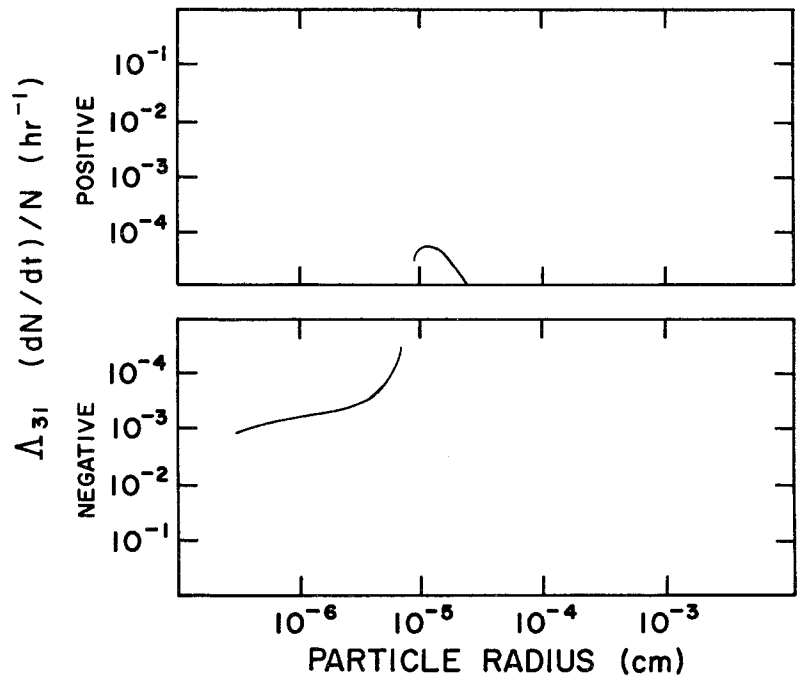

Fig. 14 Thermal coagulation of $n_3(r)$ particles

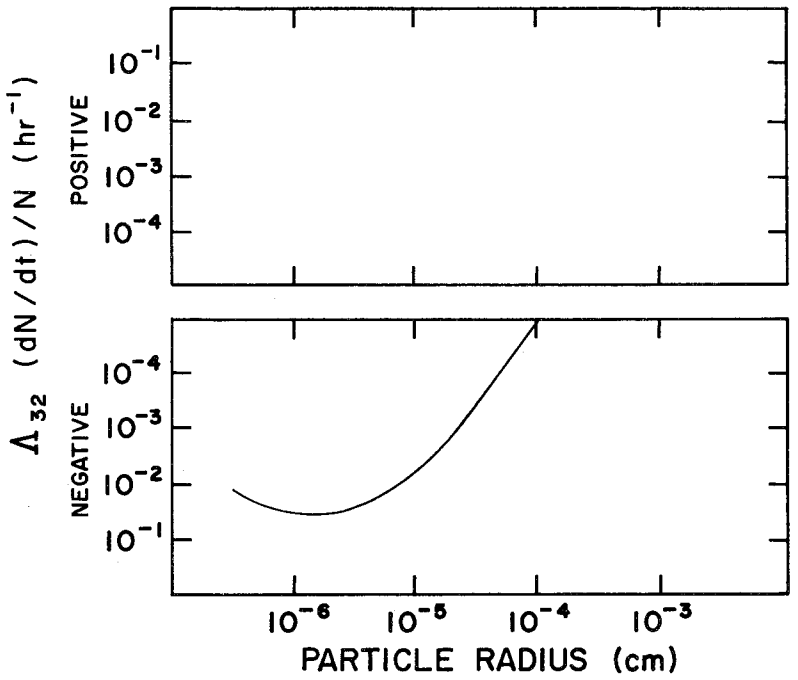

Fig. 15 Coagulation of $n_3(r)$ particles with cloud droplets

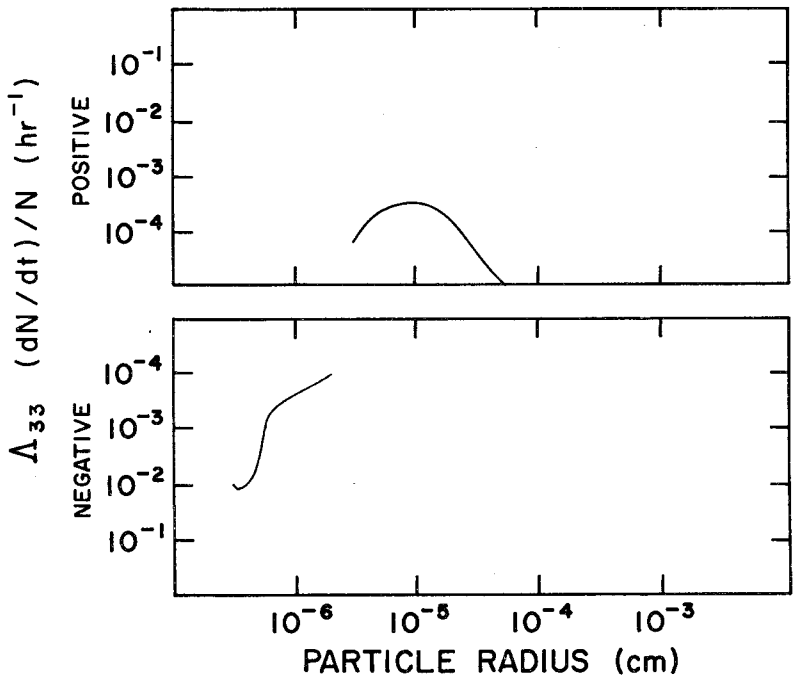

Fig. 16 Heterogeneous gas reactions, $n_3(r)$ particles

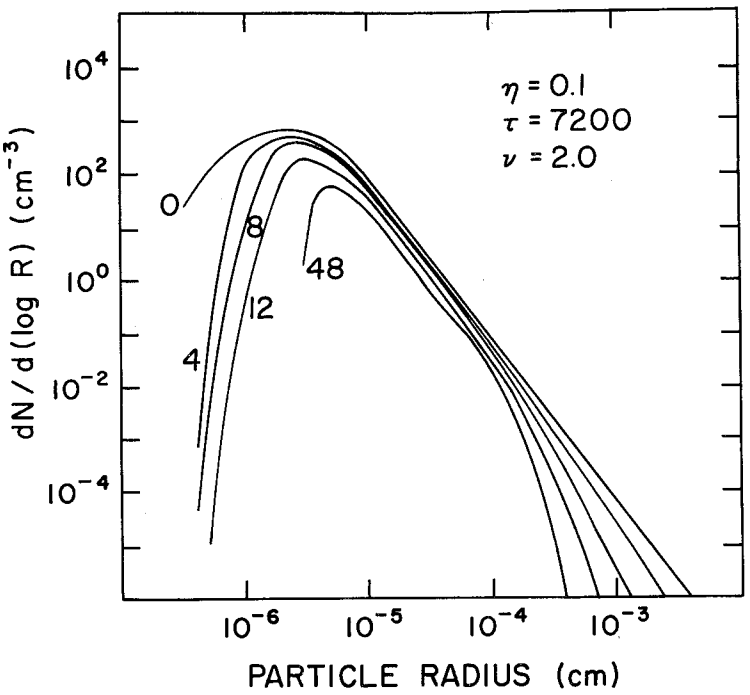

Fig. 17 All processes combined, troposphere model (time in hours)

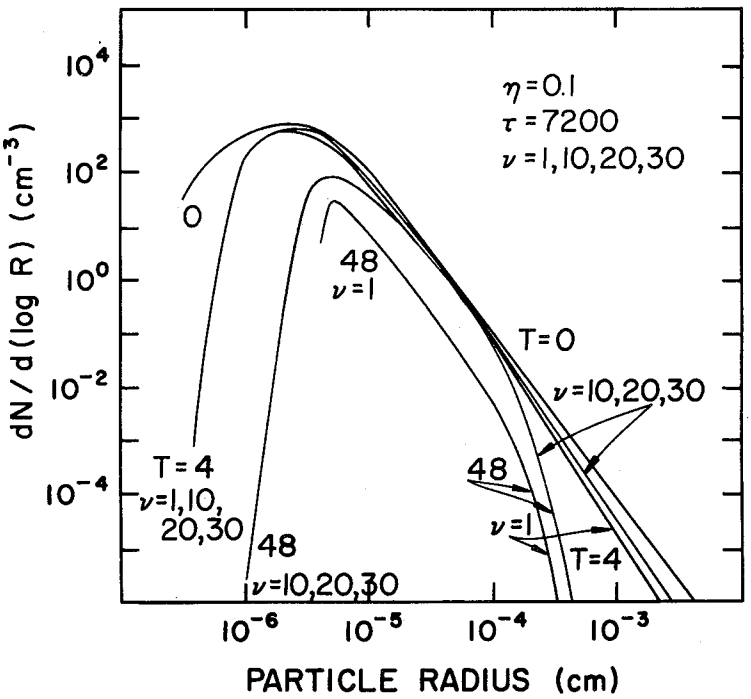

Fig. 18 Effect of varying parameter ν, troposphere model (time in hours)

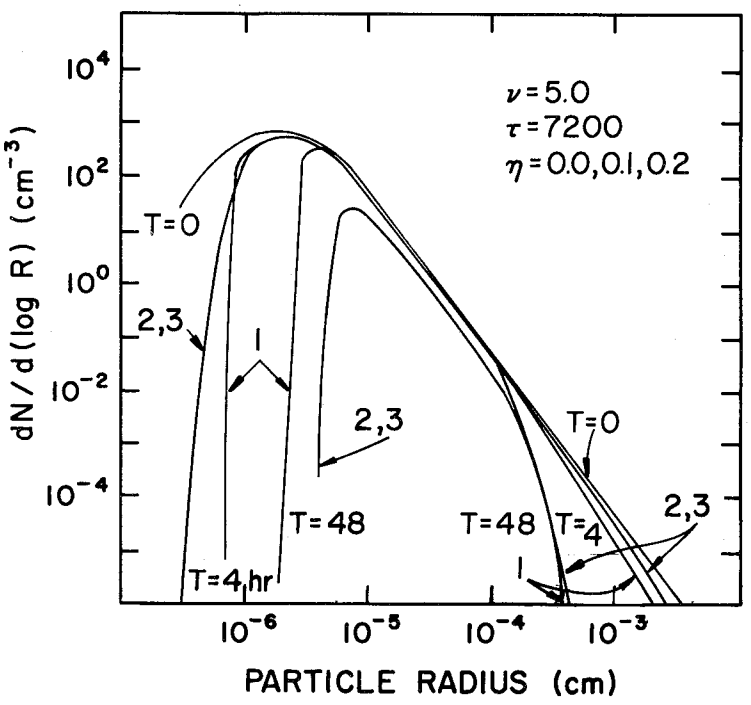

Fig. 19 Effect of varying parameter η, troposphere model (time in hours): curve 1, n = 0.0; curve 2, n = 0.1; curve 3, η = 0.2

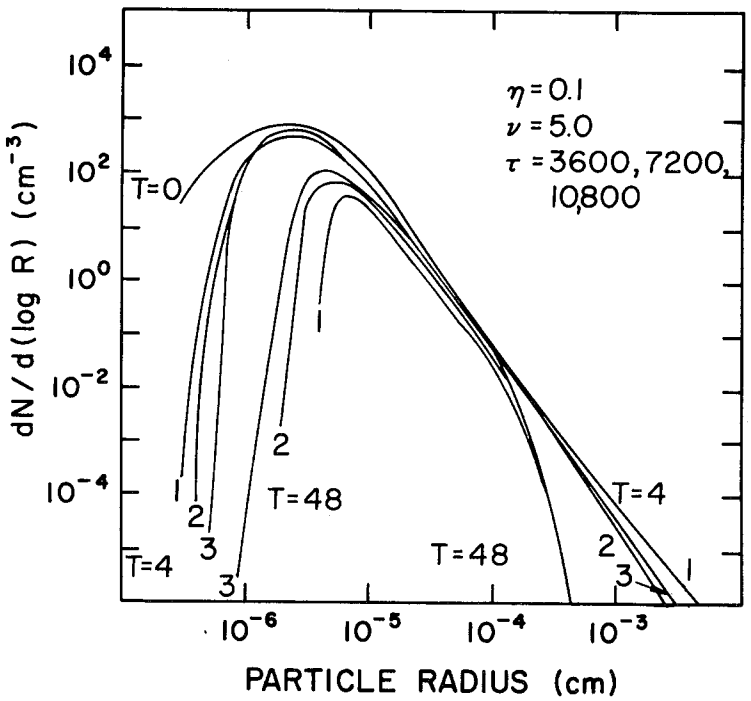

Fig. 20 Effect of varying parameter τ, tropopause model (time in hours): curve 1, τ = 36000; curve 2, τ = 7200; curve 3, τ = 10,800

APPENDIX

In this appendix we give some of the checks we have made to verify the calculations.

Of the coagulation options (11, 12, 13), only 13--shear flow coagulation--is amenable to analysis suitable for manual checking. The coagulation kernel for this option is

$$K_{SH}(r,\rho) = c(r + \rho)^3$$

We assume that $n(r,0) = b/r^4$, b constant and also that $r_a << r$. With these assumptions, the equation for option 13 becomes

$$n_1(r,\Delta t) = n(r,0) + cb^2\Delta t \left\{ \int_{r_a}^{r/\sqrt[3]{2}} (\sqrt[3]{r^3 - \rho^3} + \rho)^3 \frac{r^2\, d\rho}{\rho^4 (r^3 - \rho^2)^{2/3}} \right.$$

$$\left. - \frac{1}{r^4} \int_{r_a}^{r_b} (r + \rho)^3 \frac{d\rho}{\rho^4} \right\}$$

Expanding the cubed quantities leads to integrals which can be found by using Taylor's series for $(1 - x)^{-\alpha}$. The series obtained after integration can be summed and the result is

$$n_1(r,\ t) = n_1(r,0) + cbn_1(r,0)\left\{ \frac{r^3}{3r_b^3} + \frac{3r^2}{2r_b^2} + \frac{3r}{r_b} + \ln\frac{r^2}{r_a r_b} + \frac{4r_a}{r} - \frac{1}{3} \right\}$$

(We ignored all quantities of order $(r_a/r)^2$ in obtaining this result.)

From this information, $\Lambda_{13}(r,\Delta t)$ is easily found and can be compared with the computer results. We did this and got excellent agreement, provided we satisfied $r >> r_a$.

Options 14 and 15--the gas reactions--can be checked simultaneously We have

$$n_1(r_i,\ t + \Delta t) = n_1(r_i - \Delta r,\ t)$$

where Δr is either Δr_1 or Δr_1^*. We shall assume that Δr is small enough that

$$r_{i-1} < r_i - \Delta r < r_i$$

a condition satisfied by the larger r_i's. We used linear interpolation on $\log n_1(r_i - \Delta r,\ t)$, considered as a function of $\log r$. Doing this, and using $\log (1-x) = - x/\ln 10$ for small x, we get

$$n_1(r_i - \Delta r,\ t) = n_1(r_{i-1},\ t) \left[\frac{n_1(r_i,t)}{n_1(r_{i-1},t)}\right]^{1-\varepsilon_i}$$

where

$$\varepsilon_i = \Delta r/(r_i \ln r_i/r_{i-1})$$

Now ε_i is small compared to unity, so we use $a^{1-x} \simeq a - ax \ln a$ for small x. This gives

$$n_1(r_i - \Delta r, t) = n_1(r_i, t) \left\{ 1 - \varepsilon_i \ln \frac{n_1(r_i, t)}{n_1(r_{i-1}, t)} \right\}$$

We finally assume that the coefficient of ε_i in this equation varies slowly with t and consequently we can replace t with 0 in this factor. Then, defining

$$\rho_i = - \varepsilon_i \ln \frac{n_1(r_i, 0)}{n_1(r_{i-1}, 0)}$$

we have

$$n_1(r_i, k\Delta t) = (1 + \rho_i)^k \, n_1(r_i, 0)$$

If $t = k\Delta t$ is not too large, $(1 + \rho_i)^k = 1 + k\rho_i$ is a good approximation. Using this in the rate constant $\Lambda_{14,15}$ gives

$$\Lambda_{14,15} = \frac{3600(1 - \eta)}{\Delta t} \rho_i$$

Consequently, the rate constants for these two processes change very slowly with time and are given approximately by the above formula. Since $0 < \rho_i < 10^{-10}$, this equation is valid for moderate size $k(t=k\Delta t)$. The actual computations did change quite slowly with t and were in excellent agreement with the numbers predicted by these approximations.

For option 16, let T_R denote the rain period--i.e., rainout occurs at times which are multiples of T_R. Then

$$n_1(r_i, kT_R) = n_1(r_i, 0) \quad [1 - w(r_i)]^k$$

where

$$w(r) = \delta\left(1 - e^{-\sigma(r)}\right)$$

and

$$\delta = \frac{bh}{(1 - \eta)\overline{H}} \quad , \quad \sigma(r) = \frac{3T_R p_h \xi(r)}{4b}$$

$\xi(r)$ being the collection efficiency for raindrops. Thus

$$\Lambda_{16} = \frac{3600(1 - \eta)}{kT_R}\left[1 - \left(\frac{1}{1 - w(r_i)}\right)^k\right]$$

and values computed this way compared favorably with those generated by the programs.

For option 17, the equation for n_1 is

$$n_1(r_i, t + \Delta t) = n_1(r_i, t)e^{-V(r_i)\Delta t/\overline{H}}$$

This gives

$$n_1(r,t) = n_1(r,0)e^{-V(r)t/\overline{H}}$$

This in turn gives a theoretical rate constant of

$$\Lambda_{17} = \frac{3600(1 - \eta)}{t}\left[1 - e^{V(r)t/\overline{H}}\right]$$

Once again, the actual and theoretical results were very close.

Option 18 is the same as option 17; as expected, agreement was again good.

For option 21, the coagulation coefficient is constant, and if we assume as before that $n_2(r,0) = b/r^4$, then

$$n_2(r,\Delta t) = b^2\hat{K}\Delta t\left\{ \int_{r_a}^{r/\sqrt[3]{2}} \frac{d\rho}{\rho^4[r^3 - \rho^3]^2} + \frac{1}{3r^4}\left[\frac{1}{r_b^3} - \frac{1}{r_a^3}\right]\right\} + n_2(r,0)$$

where $\hat{K}$ is the constant coagulation coefficient. The integral can be done yielding

$$n_2(r,\Delta t) = bK\Delta t\ n_2(r,0)\ \frac{1}{r^3}\left(\frac{r^3}{3r_b^3} - \frac{1}{3} + 2\ \ln\frac{r}{r_a} - \frac{r_a^3}{3r^3}\right) + n_2(r,0)$$

Let

$$g(r) = \left[\frac{r^3}{3r_b^3} - \frac{1}{3} + 2\ \ln\frac{r}{r_a} - \frac{r_a^3}{3r^3}\right] r^3$$

Then

$$\Lambda_{21}(r,\Delta t) = \frac{3600\ b\hat{K}\ g(r)}{\frac{1}{\eta\kappa(r)} + b\hat{K}\Delta t\ g(r)}$$

Since $b \simeq 2 \times 10^{-13}$, $\hat{K} \simeq 3 \times 10^{-6}$, $1/\eta\kappa(r) \simeq 5$ for the larger r's and $0 < g(r) < 10^{13}$, we can ignore the second term in the denominator of Λ_{21} in comparison to the first. Thus

$$\Lambda_{21}(r,\Delta t) \simeq 3600\eta\kappa(r)\ b\ \hat{K}\ g(r)$$

In g(r), the value of r_a must be taken as the cut-off value in order to justify using $n_3(r,0) = b/r^4$. Even with this larger value, the numbers for Λ_{21} obtained by this approximation agreed very well with the computer generated values.

Options 22-25 are similar to options 14, 15. Consequently

$$n_2(r,k\Delta t) = [1 + \hat{\rho}_i\ ]^k\ n_2(r,0)$$

where

$$\hat{\rho}_i = \frac{\Delta r_2}{r_i\ \ln 10\ \log\ r_i/r_{i-1}}\ \ln \frac{n_2(r_{i-1},\ 0)}{n_2(r_i,\ 0)}$$

The assumptions were that $\hat{\rho}_i << 1$, $\Delta r_2 << r_i$ and the quantity $\ln[n_2(r_i,t)/n_2(r_{i-1},\ t)]$ varied slowly with t.

Ignoring powers of $\hat{\rho}_i$ larger than the first, we find

$$\Lambda_j(r_i,\ k\Delta t) = \frac{3600\eta}{\Delta t} \kappa\ (r_i)\hat{\rho}_i$$

this holding for "moderate values of k" - e.g., $k \leq 20$. Let

$$\theta_i = \frac{3600\eta}{\Delta t}\kappa(r_i)\ \frac{\hat{\rho}_i}{\Delta r_2} = \frac{3600\eta}{\Delta t}\ \ln\frac{[n_2(r_i,0)/n_2(r_{i-1},0)]}{r_i\ \ln 10\ \ln\ r_i/r_{i-1}}$$

then

$$\Lambda_j(r_i,\ k\Delta t) = \theta_i\Delta r_2(r_i)\quad ,\quad j = 22,\ \ldots\ ,\ 25$$

This shows the rates are nearly constant in time, and provides an easy means for checking the four processes involved. Comparisons were good.

Option 33 is a repeat of the ones just discussed. We obtained the approximation

$$\Lambda_{33}(r_i, k\Delta t) = \frac{3600\eta a^2}{\Delta t r_i^2} \tilde{\rho}_i$$

where

$$\tilde{\rho}_i = \frac{\Delta r_2^*}{r_i \ln 10 \log r_i/r_{i-1}} \ln \frac{n_3(r_{i-1}, 0)}{n_3(r_i, 0)}$$

and a is the "cut-off value in κ: $\kappa(r) = \exp(-(a/r)^2)$. As before, agreement was excellent.

BIBLIOGRAPHY

Blifford, I. H., 1970: Tropospheric aerosols. *J. Geophys. Res. 75*, 3099-3103.

Blifford, I. H., and L. D. Ringer, 1969: The size and number distribution of aerosols in the continental troposphere. *J. Atmos. Sci. 26*, 716-726.

Dinger, J. E., H. B. Howell, and T. A. Wojciechowski, 1970: On the source and composition of cloud nuclei in a subsident air mass over the North Atlantic. *J. Atmos. Sci. 27*, 791-797.

Friedlander, S. K., 1965: The similarity theory of the particle size distribution of the atmospheric aerosol. *Aerosols-Physical Chemistry and Applications*, (K. Spurny, Ed.), Gordon and Breach, New York.

Fuchs, N. A., 1964: *The Mechanics of Aerosols*, Macmillan Publishing Co., New York.

Gillette, D. A., and I. H. Blifford, 1971: Composition of tropospheric aerosols as a function of altitude. *J. Atmos. Sci. 38*, 1199-1210.

Goldsmith, P., H. J. Delafield, and L. E. Cox, 1963: The role of diffusiophoresis in the scavenging of radioactive particles from the atmosphere. *Quart. J. R. Met. Soc. 89*, 43-61.

Jaenicke, R., 1971: Survey of work at Mainz on aerosol size distribution. In *Proc. of the First Aerosol Modeling Symposium*, National Center for Atmospheric Research, (I. H. Blifford, Ed.), Technical Note NCAR TN/PROC-68, 27-30.

Junge, C. E., 1964: *The Modification of Aerosol Size Distribution in the Atmosphere*, Final Tech. Rept. on Contract No. Da91-591-EVC-2979 Meteorologisch-Geophysikalisches Institut der Johannes Gutenberg-Universität, Mainz, Germany.

———, 1969: Concentration and size distribution measurements of atmospheric aerosols and a test of the theory of self-preserving size distributions. *J. Atmos. Sci. 26*, 603.

———, and H. Abel, 1965: *Modification of Aerosol Size Distribution in the Atmopshere and Development of an Ion Counter of High Sensitivity*, Final Tech. Rpt. on Contract No. Da91-591-EVC-3404 Meteorologisch-Teophysikalisches Institut der Johannes Gutenberg-Universität Mainz/Germany.

———, and R. Jaenicke, 1971: New results in background aerosols from studies from the Atlantic Expedition of the *R. V. Meteor*, Spring 1969. *Aerosol Sci. 2*, 305-314.

———, E. Robinson, and F. L. Ludwig, 1969: A study of aerosols in Pacific air masses. *J. Appl. Met. 8*, 340-347.

Maxon, B. J., 1957: *The Physics of Clouds*, Oxford University Press, London and New York.

Ranz, W. E., and J. B. Wong, 1952: Impaction of dust and smoke particles on surface and body collectors. *Ind. and Eng. Chem. 44*, 1378-1381.

Tanaka, M., 1966: *On the Transport and Distribution of Giant Sea-Salt Particles Over Land (I) Theoretical Model; Special Contributions*, Geophysical Institute, Kyoto University, 6, 47-57.

Toba, Y., 1965: On the giant sea salt particles in the atmosphere (2), theory of the vertical distribution in the 10 m layer over the ocean. *Tellus 17*, 365-382.

Whitby, K. T., 1971: New data on urban aerosols and formation mechanism. In *Proc. of the First Aerosol Modeling Symposium*, National Center for Atmospheric Research, (I. H. Blifford, Ed.), Technical Note NCAR TN/PROC-68, 3-12.

Winkler, P., 1970: *Zuzammensetzung und Feuchtwachstum von Atmosphärischen Aerosolteilichen*. Dissertation, Johannes Gutenbert Universität, Mainz, Germany.